Experimental parametrization of magma mixing : application to the 1530 AD eruption of La Soufrière, Guadeloupe (Lesser Antilles)

M. PICHAVANT[1*], S. POUSSINEAU[1], P. LESNE[1], C. SOLARO[2] and J.-L. BOURDIER[1]

[1] Université d'Orléans, ISTO, UMR 7327, 45071, Orléans and CNRS/INSU, ISTO, UMR 7327, 45071 Orléans and BRGM, ISTO, UMR 7327, BP 36009, 45060 Orléans, France

[2] Université Paris Diderot 7, Institut de Physique du Globe de Paris (IPGP), 1 rue Jussieu, 75238 Paris Cedex 05, France

* Corresponding author. E-mail: pichavan@cnrs-orleans.fr

The Author 2018. Published by Oxford University Press. All rights reserved. For Permissions, please e-mail: journals.permissions@oup.com

Downloaded from https://academic.oup.com/petrology/advance-article-abstract/doi/10.1093/petrology/egy030/4938631
by CNRS - ISTO user
on 19 March 2018

ABSTRACT

New petrological data on eruption products and experimental results are integrated and a model for the evolution of the La Soufrière (Guadeloupe, Lesser Antilles arc) magma reservoir prior to the 1530 AD eruption is presented. In comparison with recent volcanic crises in the Antilles, the 1530 AD eruption is distinctive. The eruptive pyroclastic sequence shows a continuous zonation in whole-rock composition from silicic (~ 62 wt% SiO_2) to mafic andesite (~ 55 wt% SiO_2). Mafic products are estimated to be 80% of the total eruption volume. All juvenile clasts are crystal-rich (46-60 vol.% phenocrysts), the crystallinity being inversely correlated with the bulk-rock SiO_2 content. The phenocryst assemblage (plagioclase, orthopyroxene, clinopyroxene, magnetite) is constant throughout the sequence. Complexly zoned crystals are encountered, but An_{60-65}, En_{56-59} and Mt_{66-68} compositions occur in all samples. Glass inclusions are rhyolitic with up to 5-5.5 wt % H_2O. Matrix glasses are strongly heterogeneous, from ~64 to > 76 wt % SiO_2. The pre-eruptive evolution of the reservoir is dominated by the remobilization of a resident andesitic body following the arrival of a basaltic magma batch. Conditions of early remobilization are constrained from experiments on a basalt from the L'Echelle scoria cone. The arrival magma is a crystal-poor, moderately hot (975-1025°C), wet (> 5 wt % H_2O) and oxidized (NNO+1) low-MgO high alumina basalt similar to those involved in other Antilles volcanic centers. Geothermometry and experiments on a silicic andesite product of the eruption show that, for melt H_2O contents between 5 and 5.5 wt %, phenocrysts and interstitial melt in the resident magma were in mutual equilibrium at ~875°C and NNO+0.8. However, matrix glass and glass inclusion compositions show that, locally, the andesite body was as cold as 825°C. Melt volatile concentrations imply a minimum depth for the magma reservoir between 5.6 and 7.1 km, and the absence of amphibole phenocrysts indicates a maximum depth at 8.5 km. The 1530 AD eruption tapped an hybrid magma assembled by mixing approximately equal proportions of resident andesite and arrival basalt. Mineralogical indicators of the mixing event include An-rich layers in plagioclase, En-rich rims on orthopyroxene and core-rim zonation in magnetite, but overall phenocrysts were little modified during assembly of the hybrid magma. In comparison, matrix glasses were more severely affected. Mixing proceeded essentially by the addition of a mafic melt to the andesite body. The continuous chemical zonation observed in 1530 AD eruption products reflects mixing between three components (mafic melt, silicic melt, phenocryst assemblage). Timescales measured on different eruptive products range from several thousand years (U-Th-Ra disequilibria), 10s days (diffusion modelling in orthopyroxenes) to 10s hours

Downloaded from https://academic.oup.com/petrology/advance-article-abstract/doi/10.1093/petrology/egy030/4938631
by CNRS - ISTO user
on 19 March 2018

(heterogeneous matrix glasses). Short timescales since mafic recharge, lack of extensive transformations of phenocrysts, continuous whole-rock chemical zonation and predominance of mafic products are all consistent with triggering of the 1530 AD eruption by a major mafic recharge event which originated in the middle to lower Lesser Antilles arc crust.

Keywords: Antilles, Guadeloupe, La Soufrière volcano, andesite, magma mixing, experiments, timescales

INTRODUCTION

Recent volcanic crises in the Lesser Antilles arc have had major societal and economic impacts, as demonstrated by the ongoing eruption at Soufrière Hills, Montserrat (Kokelaar, 2002) and, previously, by the 1976 event at La Soufrière, Guadeloupe (Tazieff, 1977; Feuillard *et al*., 1983). Island arc volcanoes exhibit a large diversity of eruptive styles, making risk assessment particularly difficult. It is generally accepted that degassing in the conduit controls whether the eruption is explosive or effusive (e.g., Jaupart & Allègre, 1991; Martel *et al*., 1998). However, magma physical and chemical properties are for the most part acquired at greater depths (e.g., Pichavant *et al*., 2002). Therefore, eruption models require a detailed knowledge of pre-eruptive conditions in the feeding system, as well as of how they evolve in space and time.

La Soufrière, Guadeloupe, has received relatively little attention compared to neighbouring volcanoes Mt. Pelée, Martinique, and Soufrière Hills, Montserrat. Eichelberger (1978) described some samples from La Soufrière and emphasized mixing processes between mantle and crustal melts. The 1530 AD eruption of La Soufrière, which is currently viewed as a model in case of a future magmatic reactivation of the volcano (Boudon *et al*., 2008), was first described by Semet *et al*. (1981). The succession of events and the eruptive sequence were interpreted to reflect the tapping of a silicic magma body remobilized by the intrusion of a mafic magma batch (Semet *et al*., 1981). However, pre-eruptive parameters and magmatic timescales were not precisely determined (Semet *et al*., 1981). Recently, Boudon *et al*. (2008), on the basis of new field observations, radiocarbon ages and analyses of erupted products, proposed a new age (1530 AD, previously 1440 AD, Boudon et al., 1988), as well as a new scenario for the eruption. A study of U-series nuclides has emphasized the longevity

Downloaded from https://academic.oup.com/petrology/advance-article-abstract/doi/10.1093/petrology/egy030/4938631
by CNRS - ISTO user
on 19 March 2018

(up to tens of thousands of years) as well as the composite nature of the La Soufrière magma reservoir (Touboul *et al*., 2007).

Building on these studies, the present study aims at reconstructing the evolution of the La Soufrière reservoir prior to the 1530 AD eruption. Arc volcanoes are fed by complex magmatic systems, defined here as a network of conduits and connected reservoirs that allow magma transfer from the upper mantle to the surface. Key information on the dynamics of such systems is provided by the compositional variability of eruption products (e.g., Hildreth, 1981; Eichelberger *et al*., 2000). For example, recent eruptions of Mt. Pelée (1902, 1929) and Soufrière Hills (1995 to present) have yielded silicic andesite products. Both volcanoes tapped nearly homogeneous andesitic reservoirs, the magma compositional diversity being only expressed by mafic enclaves, which are indicative of basaltic recharge (Martel *et al*., 1998; Eichelberger *et al*., 2000; Murphy *et al*., 2000; Pichavant *et al*., 2002). For the 1530 AD eruption of La Soufrière, mafic recharge of the reservoir has also been suggested (Semet *et al*., 1981; Boudon *et al*., 2008), but the compositional variability is expressed quite differently from that at Mt. Pelée and Soufrière Hills: (1) The La Soufrière 1530 AD eruptive sequence shows a remarkably continuous zonation in whole-rock compositions, from silicic (~ 62 wt % SiO_2) to mafic andesite (~ 55 wt % SiO_2, Semet *et al*., 1981; Poussineau, 2005; Boudon *et al*., 2008); (2) Mafic products are largely predominant (proportion estimated at 80% of the total eruption volume, Semet *et al*., 1981; Poussineau, 2005); (3) Mixing and mingling between magmas of contrasted compositions are documented by black-and-white banded pumices which form a distinctive juvenile component of the eruption (Semet *et al*., 1981; Poussineau, 2005; Boudon *et al*., 2008); (4) At smaller scales, mixing is also marked in phenocrysts, i.e., by sieve-textured plagioclases and inversely zoned orthopyroxenes (Semet *et al.*, 1981; Poussineau, 2005); (5) U-Th-Ra disequilibria show that old cumulates were recycled in the erupted magmas (Touboul *et al*., 2007). All these features point to a specific mechanism of mafic magma recharge in the La Soufrière reservoir. Here we define the characteristics of the mixing event that preceded the 1530 AD eruption and, in particular, we quantify: (1) the *gradients* (both chemical and physical, i.e., concerning the pre-eruptive parameters) and (2) the *timescales* associated with this event.

To achieve these objectives, petrological results, both on natural eruption products and experiments, are combined below. New analytical data for phenocrysts and glasses (including glass inclusion H_2O concentrations) are presented to complement the database for the 1530 AD eruption products (Semet *et al*., 1981; Poussineau, 2005; Boudon *et al*., 2008). Experimental data are provided to constrain the conditions of the silicic and mafic magmas

Downloaded from https://academic.oup.com/petrology/advance-article-abstract/doi/10.1093/petrology/egy030/4938631
by CNRS - ISTO user
on 19 March 2018

involved in the eruption. A dynamic model for the evolution of La Soufrière reservoir is constructed which emphasizes the short timescales associated with the mixing event preceding the 1530 AD eruption.

LA SOUFRIÈRE VOLCANO

In Guadeloupe, the southern part of Basse-Terre comprises several calc-alkaline volcanic edifices of Pleistocene to Recent age (Dagain *et al*., 1981; Samper *et al*., 2009) built on a pre-Miocene volcanic basement (Fig. 1). The La Soufrière volcano, located at the south of the island (Tazieff, 1977; Feuillard *et al*., 1983) is currently active (e.g., Allard *et al*., 2014). The building of the Grande Decouverte – La Soufrière composite volcano is conveniently divided into three main periods (see Boudon *et al*., 2008 and references therein; Samper *et al*., 2009). The *first* period ("Grande Decouverte" stage) extends from 0.25 Ma to 42 kyr. It comprises an alternation of effusive and pyroclastic episodes of andesitic composition. It ended with a major pumiceous event (known as "Pintade", dated at 42,350 yr, see Boudon *et al*., 2008), which represents the greatest plinian episode of the volcano and led to the formation of the Grande Decouverte caldera. The *second* period corresponds to the "Carmichael" phase from 42 to 11.5 kyr. The construction of the Carmichael massif took place inside the Grande Decouverte caldera (Boudon *et al*., 2008). This eruptive phase consists of predominantly lava flows plus domes associated with pyroclastic activity. It ended with two major flank collapse events at 13.5 and 11.5 kyr BP (Boudon *et al*., 2008 and references therein). The *third* (and current) period is the "La Soufrière" phase from 11,500 yr BP to present, and it corresponds to the activity of the La Soufrière volcano *ss*. Volcanic activity, centered roughly on the current dome, has led chronologically to the formation of the Amic lava dome, the construction of the two scoria cones of L'Echelle and La Citerne (~ 1700 yr BP, see Boudon *et al*., 2008) and, finally, to the construction of the La Soufrière lava dome during the last major magmatic eruption of the volcano (1530 AD, Boudon *et al.*, 2008). Since then, the volcanic activity has been marked exclusively by phreatic eruptions, the last one in 1976-1977 (Tazieff, 1977; Feuillard *et al*., 1983; Allard *et al*., 2014).

The eruption considered in detail in this study is that of 1530 AD. Following Vincent *et al.* (1979), Dagain *et al.* (1981) and Boudon *et al.* (1988), the eruptive scenario has been recently updated (Boudon *et al*., 2008). The eruption began with a phreatic event that produced a fine ash fallout deposit. Magma arrived just after at the surface and triggered a

Downloaded from https://academic.oup.com/petrology/advance-article-abstract/doi/10.1093/petrology/egy030/4938631
by CNRS - ISTO user
on 19 March 2018

low-volume flank collapse that increased the magma discharge and led to a sub-plinian phase. Silicic andesite magma emitted as white pumice at the onset of the eruption rapidly evolved to mafic andesite magma, with a transition marked by spectacularly banded black and white pumice clasts. The eruption then changed its eruptive style with the fallout of coarse dark mafic andesite scoriae generated as a result of strombolian-like lava fountaining. The end of the eruption was marked by the growth of the La Soufrière lava dome from degassed magma compositionally similar to the most mafic scoriae.

METHODS

Natural samples

This study is based on three sets of natural samples (Supplementary Data Table s1). Petrological work was initially carried out on a first set of 1530 AD samples collected in 2000 (Boudon *et al.*, 2008). Information about the locations and stratigraphic relationships of these samples can be found in Boudon *et al.* (2008). From this first set, four samples were studied in detail, i.e., white and dark layers from a banded juvenile pumice (O1215Eb, O1215Ea), a grey homogeneous pumice from the base of the deposit (O1215B2) and a dark homogeneous scoria (O1215G). A second set (25 in total) of 1530 AD samples was collected in 2002 from sections (0.5 to ~3 m high) NE of the La Soufrière dome, near the Carbet Spring section of Boudon *et al.* (2008). Three samples, a banded pumice (SG11A) and two white-grey homogeneous pumices from the base of the deposit (SG5A-2, SG7B-1), were studied in detail. The third sample set, which exclusively concerns mafic rocks, comprises both old (N. Metrich and M. Semet, personal communications, Dagain *et al*., 1981) and new samples, the latter collected from the La Soufrière dome and the nearby L'Echelle scoria cone. Two mafic scoriae, one from the La Soufrière dome (SG3) and the other from L'Echelle (GW4O) were studied in detail.

Analytical methods

A limited number of whole-rocks were analysed (five homogeneous 1530 AD white-grey andesitic pumices, two mafic scoriae), essentially for comparison with previous data (Dagain *et al*., 1981; Semet *et al*., 1981; N. Metrich and M. Semet, personal communications, 2004; Boudon *et al.*, 2008). Once crushed and powdered, the samples were analysed by ICP-AES (SARM, CRPG, Vandoeuvre les Nancy).

Downloaded from https://academic.oup.com/petrology/advance-article-abstract/doi/10.1093/petrology/egy030/4938631
by CNRS - ISTO user
on 19 March 2018

Petrological studies were carried out both on 1530 AD and L'Echelle samples. To complement previous results (Semet *et al*., 1981; Boudon *et al*., 2008), focus was placed on compositional gradients in phenocrysts, glass inclusions and matrix glasses and on H_2O concentrations. Modal compositions (previously estimated by mass-balance, Touboul *et al*., 2007; Boudon *et al*., 2008) were determined by point counting. Only crystals larger than 100 μm were counted as phenocrysts.

Both natural samples and experimental charges were examined by scanning electron microscopy (SEM). Different instruments, a JEOL JSM-6400 (Polytech, Orléans) and a Zeiss Merlin Compact microscope (ISTO, Orléans) operated at 15-20 kV and 15 kV acceleration voltage, respectively, were successively used. Crystals (either natural or experimental) were analysed by electron microprobe. Both spot analyses, compositional profiles (steps of 3 to 5 μm) and element X-ray distribution maps were obtained using successively a Cameca Camebax microbeam, a Cameca SX50 and a Cameca SX Five (BRGM-CNRS laboratory, Orléans). Analytical conditions were 6-12 nA sample current, 15 kV acceleration voltage, 1-2 μm beam size and 10 s counting time on peak.

Preliminary modelling for Fe-Mg interdiffusion in orthopyroxene was performed by intercalibration of high resolution BSE-images with microprobe data, to obtain effective Mg-number with high spatial (~500 nm) and analytical (~0.2 mol%) resolution (Allan *et al*., 2013; Solaro 2017). The diffusion calculations were performed along the a-axis of crystals using the diffusion coefficient of Ganguly & Tazzoli (1994), assumed to be independent of fO_2 (Dohmen *et al*., 2016). Temperatures were set at 900 and 950°C (more fully justified below). Profiles were modeled with open boundary conditions (i.e., exchange between crystal and melt) and sharp step-wise initial conditions (i.e., instantaneous growth followed by diffusion).

Glasses (1530 AD and experimental samples) were analysed only with the SX50 and SX Five electron microprobes; the sample current was set to 6 nA and the beam was defocused to either 5x5 μm or 10x10 μm. Alkali migration was corrected for empirically by analysing secondary hydrous glass standards of known Na and K contents (Pichavant, 1987; Scaillet *et al*., 1995). For glass water contents of 5-6 wt %, typical correction factors were ~5% for Na and $\leq$1% for K (Poussineau, 2005). Average analytical errors on electron microprobe data are 1% relative for SiO_2 and Al_2O_3, 2% for CaO, 3% for FeO, MgO and TiO_2 and 5% for MnO, Na_2O and K_2O.

A modified "by difference" method (Devine *et al*., 1995) was used to estimate the water content of matrix glasses, glass inclusions (1530 AD samples only) and experimental glasses. Differences from 100% of glass electron microprobe analyses were calibrated against

Downloaded from https://academic.oup.com/petrology/advance-article-abstract/doi/10.1093/petrology/egy030/4938631
by CNRS - ISTO user
on 19 March 2018

4 rhyolitic standard glasses containing between 0 to 6 wt % H_2O, as determined by Karl-Fisher titration and ion microprobe (Scaillet *et al*., 1995; Martel, 1996). With this modified method, errors on H_2O estimations are reduced to $\pm$ 25% relative (Poussineau, 2005). H_2O concentrations in glass inclusions were also determined by FTIR. The spectra were obtained with a Magna 760 NICOLET™ spectrometer (ISTO, Orléans) attached to a NICPLAN microscope and equipped with an automatic dry air purge. Data acquisition was performed using a white lamp, a CaF_2 beam-splitter and a MCT-A detector. Spectra were collected between 2000 cm^{-1} and 6000 cm^{-1} with a resolution of 2 cm^{-1} and accumulated for 128 scans. The size of the infrared beam was varied between 30 and 100 μm. Thicknesses of doubly polished host crystals were determined with a micrometer coupled to an optical microscope. Glass densities were measured and absorption coefficients determined (5230 cm^{-1} (ε_{H2O}): 1.75 $L.mol^{-1}.cm^{-1}$, 4500 cm^{-1} (ε_{OH}): 1.35 $L.mol^{-1}.cm^{-1}$) by using 5 hydrous rhyolitic standard glasses, using procedures detailed in Poussineau (2005). Total glass water concentrations were obtained by adding molecular H_2O and hydroxyl group concentrations determined from the Beer-Lambert law applied to the 5230 and 4500 cm^{-1} absorption bands (Stolper, 1982; Silver & Stolper, 1989; Ohlhorst *et al*., 2001).

Experimental methods

Strategy and starting samples

Pre-eruptive physical parameters (temperature, melt water content, pressure of magma storage, redox conditions, volatile fugacities) can be precisely defined from experimental phase equilibria (Rutherford *et al*., 1985; Barclay *et al*., 1998; Martel *et al*., 1998; 1999; Scaillet & Evans, 1999; Costa *et al*., 2004; Scaillet *et al*., 2008). Because of marked chemical gradients in the La Soufrière 1530 AD reservoir, experiments were performed separately on two samples, respectively representative of the silicic and mafic magmas prior to their interaction and mixing (see Pichavant *et al*., 2007). For the silicic magma, the most SiO_2-rich of the five homogeneous, white-grey pumices sampled at the base of the deposit (SG7B-1, Table 1) was chosen. As shown below, these basal products are representative of the silicic (andesite) end-member magma tapped during the eruption. For the mafic magma, pre-eruptive conditions were constrained from experiments on a basalt from L'Echelle. Mafic rocks from the 1530 AD products were initially considered, but finally discarded because most are macroscopically heterogeneous and contain variable amounts of crystals coming from the

Downloaded from https://academic.oup.com/petrology/advance-article-abstract/doi/10.1093/petrology/egy030/4938631
by CNRS - ISTO user
on 19 March 2018

silicic magma. The most mafic 1530 AD products are quite evolved (SiO_2 ~ 55 wt %) and they represent syn-eruptive mixtures (Semet *et al*., 1981; Boudon *et al*., 2008) rather than the mafic end-member magma. In comparison, the products from L'Echelle are more homogeneous, chemically more primitive and less contaminated by silicic magmas. Basalt GW4O (Dagain *et al.* 1981), the most mafic sample (Table 1) of the La Soufrière massif, was chosen for the experimental study. Although not a product of the 1530 AD eruption (the L'Echelle scoria cone is older), GW4O is the best representative of the mafic magmas recharging the La Soufrière reservoir.

The two experimental starting glasses were prepared by crushing and fusing twice (with grinding in between) their respective rock powders in a Pt crucible at 1400°C, 1 atm, for 3-4 hours. Then, each glass was finely ground to a 20-50 μm powder. Electron microprobe analyses show that the two glasses are chemically homogeneous and close to their respective whole-rock compositions (Table 1).

Experiments

Au capsules of 15 mm length, 2.5 mm internal diameter and 0.2 mm wall thickness were used as containers for the andesite and the basalt experiments. Deionized water, CO_2 (as silver oxalate, $Ag_2C_2O_4$) and the silicate glass powder were loaded successively in the capsule. Both water-undersaturated and water-saturated experiments were performed. The former used either H_2O-CO_2 mixtures (fluid-present conditions, initial molar $H_2O/(H_2O+CO_2) < 1$) or amounts of H_2O added < saturation (fluid-absent conditions). For the latter, pure H_2O was added to the charge in a proportion slightly exceeding saturation (fluid-present conditions). All experiments were performed in an internally heated pressure vessel pressurized with Ar-H_2 gas mixtures (Scaillet *et al*., 1992). A molybdenum furnace with two windings was used. Temperature was continuously monitored by two type K thermocouples and the temperature gradient never exceeded 5°C. Total pressure was measured to $\pm$ 2 MPa with a pressure gauge calibrated against a Heise tube manometer. A drop-quench technique was quasi-systematically used (Di Carlo *et al*., 2006), allowing quench rates of ~100°C.s^{-1} under nearly isobaric conditions. Three andesite experiments were performed with the vessel fitted with a Shaw-type semipermeable H_2 membrane (Scaillet *et al.,* 1992); these were isobarically rather than drop-quenched (quench rate ~300°C/min).

Control of redox conditions

Downloaded from https://academic.oup.com/petrology/advance-article-abstract/doi/10.1093/petrology/egy030/4938631
by CNRS - ISTO user
on 19 March 2018

The redox state of experimental charges was controlled by the fH_2 of the Ar-H_2 gas pressure medium. In most cases, experimental fH_2 were measured with Ni-Pd-O solid sensors (Taylor *et al*., 1992; Pownceby & O'Neill, 1994). Sensor capsules were run together with the other capsules in the same experiment, and the final NiPd alloy composition (X_{Ni}) was determined by electron microprobe. In three andesite experiments, experimental fH_2 was measured continuously with a Shaw membrane (Scaillet *et al*., 1992). The oxygen fugacity (fO_2) of each charge was calculated from the measured fH_2 and the fH_2O determined from the H_2O content of the experimental glasses, either estimated with the modified by-difference method or calculated (Burnham, 1979) in the case of H_2O-saturated charges. Glass in one near-liquidus basaltic charge was analysed for H_2O by Karl-Fisher titration (Pichavant *et al*., 2002; Poussineau, 2005). The model of Burnham (1979) was used to compute fH_2O from melt H_2O contents and pure H_2O fugacities were taken from Burnham *et al*. (1969). The uncertainty on $\log fO_2$ is $\pm$ 0.25 log unit (Scaillet *et al*., 1995; Martel *et al*., 1999; Pichavant *et al*., 2002).

RESULTS

1530 AD eruption products

Bulk rock and modal compositions

Representative whole-rock major element compositions of 1530 AD products are given in Table 1 and the entire data set is plotted in Fig. 2. Products from the 1530 AD eruption range continuously from mafic (55-56 wt % SiO_2) to silicic andesite (62 wt % SiO_2), and they include one dacite if the pce77 sample of Semet *et al*. (1981) is considered (Fig. 2). Concerning this latter sample, we note that the presence of dacite in the 1530 AD products has not been confirmed by recent field campaigns (Poussineau, 2005; Boudon *et al*., 2008). Moreover, pce77 does not plot in continuity with the 1530 AD data points, having abnormally low Al_2O_3 and high MgO for such a high SiO_2 content (Fig. 2). Therefore, the attribution of pce77 to the 1530 AD eruption must be questioned. The new bulk-rock analyses are in good agreement with literature data (Fig. 2). The La Soufrière 1530 AD andesites have low to medium K_2O and relatively high FeO_t/MgO, similar to most active volcanoes along the Lesser Antilles arc (Macdonald *et al*., 2000). Although the 1530 AD products lack basaltic rocks, the L'Echelle and Citerne products extend the mafic end of 1530 AD samples (Fig. 2).

Downloaded from https://academic.oup.com/petrology/advance-article-abstract/doi/10.1093/petrology/egy030/4938631
by CNRS - ISTO user
on 19 March 2018

Phenocrysts

Modal data are available for several 1530 AD samples across the bulk-rock compositional range (Table 1). All products are crystal-rich, comprising 46-60 vol.% phenocrysts. The most silicic samples (SG7B-1, O1215Eb) contain 35-36 vol.% plagioclase, 8-9 vol.% orthopyroxene, 2 vol.% clinopyroxene and 1 vol.% Fe-Ti oxides. There is no change in phenocryst assemblage from silicic to mafic andesites but the crystal content increases with decreasing bulk-rock SiO_2 content, reaching 43 vol.% plagioclase, 12 vol.% orthopyroxene and 3 vol.% clinopyroxene in scoria O1215G (Table 1). Amphibole is absent in all eruption products. Neither quartz nor olivine (see Semet *et al*., 1981; Boudon *et al*., 2008) were found in our 1530 AD samples, but olivine (Fo_{64-80}), plagioclase, clinopyroxene, orthopyroxene and Fe-Ti oxides occur in basalt GW4O (Table 1). Representative analyses of phenocrysts are given in Supplementary Data Tables s2-5.

Plagioclase is euhedral to subhedral and ranges in size from small (< 100 μm) microphenocrysts to large phenocrysts (up to about 2 mm). It shows well-developed oscillatory zoning and is typically rich in glass inclusions. Plagioclase crystals are texturally and chemically similar between samples. Growth zoning is marked by the occurrence of discrete An-rich layers superimposed on a "background" composition of ~An_{60-65} (Fig. 3; Supplementary Data Table s2). In the most silicic samples (O1215Eb and O1215B2), rim compositions are close to An_{60}, in agreement with previous data (Semet *et al*., 1981), and An-rich layers are < An_{85}. In the most mafic samples (O1215G), sieve textures are frequently encountered (Semet *et al*., 1981; Poussineau, 2005) and An-rich layers reach An_{90} (Fig. 3; see also Semet *et al*., 1981). Some of these An-rich layers were found in external positions in the crystal (in agreement with Semet *et al*., 1981), but they are always separated from the matrix by a thin, lower An rim. Plagioclase (An_{62-84}) is also the dominant phenocryst in basalt GW4O. Semet *et al.* (1981) mentioned the occurrence in the 1530 AD products of glomeroporphyritic aggregates with unzoned An_{90} plagioclase and Fo_{75} olivine.

Orthopyroxenes in the 1530 AD products form euhedral crystals, 0.2-2 mm in size. They have En mostly between 56 and 59, contain 2.5-3.5% Wo and < 1 wt % Al_2O_3 (Supplementary Data Table s3; see also Semet *et al*., 1981). Crystals with this "common" composition are found in all samples. In addition, a few more Mg-rich orthopyroxenes, up to En_{71}, occur sporadically. A few inversely zoned crystals, from En_{58-59} cores to En_{68-74} rims, have been encountered (Fig. 4, see also Semet *et al*., 1981; Poussineau, 2005) and some were used for preliminary Fe-Mg diffusion modelling (results detailed below). In GW4O basalt,

Downloaded from https://academic.oup.com/petrology/advance-article-abstract/doi/10.1093/petrology/egy030/4938631
by CNRS - ISTO user
on 19 March 2018

orthopyroxene is practically absent. Only one crystal (En_{69}) was found rimmed by clinopyroxene and is interpreted as a xenocryst coming from a silicic magma.

Clinopyroxenes, although less abundant than orthopyroxenes, are present in all studied samples (Supplementary Data Table s4). These are mostly augites ($En_{38}Wo_{42}$, Mg# = 64-66, Al_2O_3 < 2 wt %, TiO_2 < 0.5 wt %, see also Semet *et al*., 1981). Crystals with higher Mg# (68-70) occur sporadically, see also Semet *et al*. (1981). An Al- and Ti-rich (> 7 wt % Al_2O_3, ≥ 1 wt % TiO_2) Cr-bearing diopside ($En_{40}Wo_{46}$, Mg# = 73-76) rimmed by orthopyroxene of "common" composition was found in O1215G and is interpreted as a xenocryst coming from a mafic magma since clinopyroxenes with the same chemistry occur in the GW4O basalt.

Fe-Ti oxides occur in all studied samples. Both magnetite and ilmenite phenocrysts, usually < 500 μm in size, are present. Magnetite is much more abundant than ilmenite (ilmenite is very rare and sometimes absent) and is mostly homogeneous, with Mt between 66 and 68, 11-12 wt % TiO_2, 2-3 wt % Al_2O_3 and 1-2 wt % MgO (Supplementary Data Table s5; Semet *et al*., 1981). This compositional group is common to all samples. Scoria O1215G hosts strongly zoned magnetites from Mt-poor (Mt_{51}) rims to Mt-rich (Mt_{84}) cores (Poussineau, 2005). Mt-rich magnetites (Mt_{73-79}) are also present in basalt GW4O (Supplementary Data Table s5). Ilmenite compositions, determined in O1215Eb and O1215B2 only (Supplementary Data Table s5), are homogeneous (~Ilm_{75}).

Glass inclusions

Major element compositions of 1530 AD glass inclusions (MI) are given in Table 2 and plotted in Fig. 5. MI have 5-100 μm sizes, on average ~50 μm, and occur mostly in plagioclase and orthopyroxene phenocrysts. They are all rhyolitic (71.5 to 76.5 wt % SiO_2 anhydrous, Table 2; Poussineau, 2005) irrespective of the whole-rock composition. However, although the data overlap, MI compositions extend to slightly higher SiO_2 (76.5 wt %) in the most silicic (O1215Eb) than in the two other less silicic (O1215B2, O1215G) samples (71.5-75 wt %, Fig. 5). No correlation was found between the MI chemistry and the nature of the host crystal (see also Semet *et al*., 1981), suggesting no significant post-entrapment modification.

Matrix glasses

Matrix glasses in the 1530 AD products are strongly heterogeneous (Table 2). Combining our data with those of previous studies (Semet *et al*., 1981; Boudon *et al*., 2008), the total range of matrix glass SiO_2 exceeds 10 wt %, from ~64 to > 76 wt% anhydrous (Fig. 6). Matrix glass

Downloaded from https://academic.oup.com/petrology/advance-article-abstract/doi/10.1093/petrology/egy030/4938631
by CNRS - ISTO user
on 19 March 2018

SiO_2 contents are positively correlated with K_2O and negatively correlated with Al_2O_3, FeO_t, CaO and MgO. The relation between matrix glass and whole-rock compositions is complex. The most silicic (up to 82 wt % SiO_2) matrix glasses are found in an homogeneous andesitic pumice (SG7B-1, a microlite-rich sample) and in white layers of banded pumice (O1215Eb). The most mafic glasses are found in dark layers of banded pumices (O1215Ea and SG11A) and in dark scoriae (Boudon *et al*., 2008). Macroscopically homogeneous samples have sub-homogeneous matrix glasses. They become progressively less SiO_2-rich as their bulk-rock SiO_2 decreases, although microlite-rich scoriae (e.g., SG3) host quite silicic residual glasses (Table 2). In white layers of banded pumices, matrix glasses are homogeneous and nearly microlite-free, whereas in dark layers the glass is chemically heterogeneous at a small scale (< 10 μm, Fig. 7) and microlites (plagioclase, orthopyroxene and magnetite) are abundant (see also Boudon *et al*., 2008).

Glass water contents

For glass inclusions, both by difference estimations and FTIR data are available (Fig. 8). The by difference method yields 1.40-5.67 wt % H_2O in O1215Eb (13 inclusions), 1.91-5.50 wt % H_2O in O1215B2 (19 inclusions) and 0.77-5.47 wt % H_2O in O1215G (6 inclusions). The FTIR data, which were all obtained on plagioclases separated from SG5A-2 (Table s1), yield 1.67-5.32 wt % H_2O (8 inclusions, Poussineau, 2005). Both methods confirm the large range of glass inclusion H_2O concentrations and they give almost identical H_2O concentrations maxima (~ 5.5 wt %).

For matrix glasses, only by difference data are available. The average H_2O concentrations are similar for the different samples, i.e., 1.1, 0.9 and 1.0 wt % H_2O for O1215Eb (6 measurements), O1215B2 (5 measurements) and O1215G (6 measurements), respectively (Table 2). H_2O maxima in matrix glasses are in the same range as H_2O minima in glass inclusions, suggesting that the low H_2O concentrations in glass inclusions result from inclusion leakage and degassing during the eruption.

Experimental results

Basalt experiments

The experimental results on GW4O basalt are summarized in Table 3 and the experimental compositions detailed in Supplementary Data Table s6. Data are available both at 200 and 400 MPa for melt H_2O concentrations from 3 to 9.3 wt %, fO_2 from NNO-0.2 to NNO+4.1

Downloaded from https://academic.oup.com/petrology/advance-article-abstract/doi/10.1093/petrology/egy030/4938631
by CNRS - ISTO user
on 19 March 2018

and temperatures from 950 to 1038°C. Phase assemblages encountered include liquid (quenched to glass), spinel (designated below as magnetite), plagioclase, olivine, amphibole, clinopyroxene and orthopyroxene. The 200 MPa charges are crystal-rich (up to > 60% at 950°C, charge L1-1, Table 3). They systematically contain olivine, and amphibole crystallizes only at temperatures ≤ 975°C. In contrast, the 400 MPa charges generally have lower crystallinities (except for one low melt H_2O content charge, P2-5, Table 3). Olivine is rare, being found only in one 400 MPa charge (P5-13, Table 3) and amphibole has a large stability field at and below 1000°C. At 200 MPa, plagioclase (plus magnetite) is the liquidus phase, followed by olivine and clinopyroxene. At 400 MPa for melt H_2O concentrations > 6 wt %, amphibole (plus magnetite) is the liquidus phase. For lower melt H_2O contents, plagioclase replaces amphibole on the liquidus. Residual glasses become progressively more evolved with progressive crystallization, reaching ~60 wt % SiO_2 in 3 charges (L1-1, L2-1, P6-17, Table 3). Experimental plagioclases range from An_{65} to An_{89}, with An positively correlated with temperature and the melt H_2O content (see Pichavant *et al*., 2002, their fig. 8). Experimental olivines have Fo contents between 72 and 85, the two highest Fo (84, 85) being associated with oxidizing (> NNO+2) charges (Table 3). Orthopyroxene (En_{68} and En_{59}) occurs in the two most crystallized charges. In comparison, magnetite is present in all charges and covers a wide compositional range, from Mt_{97} to Mt_{43}, depending on temperature and fO_2 (Supplementary Data Table s6). Clinopyroxene (present in 4 charges) has an Mg# between 64 and 80, Al_2O_3 between 3.17 and 6.97 wt % and TiO_2 between 0.61 and 1.11 wt %. Amphibole (present in 5 charges) is pargasitic.

Andesite experiments

Experimental conditions and results are summarized in Table 4 and compositions detailed in Supplementary Data Table s7. All experiments were carried out between 100 and 200 MPa and from 800°C to 950°C. Most experiments were performed close to NNO+1 but both more reducing (ΔNNO < 0) and more oxidizing (ΔNNO > +3) conditions were also explored. Melt H_2O concentrations range from 2 to 6.9 wt %. Most charges have the same phase assemblage, including liquid (quenched to glass), plagioclase, orthopyroxene and magnetite. Clinopyroxene is common as an additional phase between 850-925°C, but is absent below 850°C and at 950°C. Amphibole is restricted to between 825°C and 800°C and ilmenite was detected in 4 reduced charges (Table 4). Crystallinities range from 13 to 81 wt % and are positively correlated with decreasing temperature and melt H_2O concentration. Experimental glasses (Supplementary Data Table s7) cover a large range, from andesitic to rhyolitic. Upon

Downloaded from https://academic.oup.com/petrology/advance-article-abstract/doi/10.1093/petrology/egy030/4938631
by CNRS - ISTO user
on 19 March 2018

decreasing temperature or melt H_2O content, or upon increasing crystallinity, glass SiO_2 and K_2O increase while Al_2O_3, FeO, MgO, and CaO decrease. Compositions of experimental plagioclases (Supplementary Data Table s7) range from An_{49} to An_{81}, and are positively correlated with temperature and melt H_2O concentration, and slightly negatively correlated with pressure. Experimental orthopyroxenes have En between 43 and 79, increasing with fO_2, melt H_2O concentration and temperature, and slightly decreasing with pressure. Magnetites have Mt from 48 to 84 and they follow the same compositional trends as orthopyroxene. Clinopyroxenes are augites with Mg# between 55 and 79 and Al_2O_3 contents between 1.3 and 8.2 wt %. Amphibole ranges from pargasite to magnesio-hornblende. Ilmenite is rich in the Ilm component (Ilm_{90-92}), consistent with the low fO_2 of the charges in which it was detected.

THE 1530 AD MAGMA RESERVOIR

Structure of the reservoir

The wide range of compositions of erupted whole-rocks, plus the textural and mineralogical evidence for mixing between andesitic and basaltic magmas, implies that the La Soufrière reservoir was strongly heterogeneous, both chemically and physically. In their influential work, Semet *et al*. (1981) proposed that the pre-1530 AD La Soufrière reservoir was remobilized following the arrival of a mafic magma batch. The continuous zonation in whole-rock compositions would imply that the eruption tapped a single magma reservoir, instead of two vertically disconnected chambers (e.g., Traineau *et al*., 1986; Fichaut *et al*., 1989; Pichavant *et al*., 2002). Although the geometries are poorly constrained, the proportions of the arrival and resident magmas can be estimated at 40 and 60%, respectively, by using the volumetric constraints provided by Semet *et al*., (1981). Below, two successive stages in the evolution of the reservoir are distinguished. The first corresponds to the arrival of the mafic magma batch and to the beginning of the chemical and physical perturbation of the andesitic body (Fig. 9a). The second represents the later, more advanced situation immediately preceding the eruption and frozen in the eruption products (Fig. 9b).

Downloaded from https://academic.oup.com/petrology/advance-article-abstract/doi/10.1093/petrology/egy030/4938631
by CNRS - ISTO user
on 19 March 2018

The basaltic magma and conditions of early remobilization

The arrival magma, represented by mafic products from L'Echelle, has a basaltic (~ 50 wt % SiO_2) composition and is very crystal-poor, as demonstrated by the nearly total lack of crystals of clear basaltic provenance in the eruption products (exceptions include olivine crystals, glomeroporphyritic plagioclase-olivine aggregates and Al-rich clinopyroxenes). Physical conditions in the arrival magma are closely simulated by the experiments on basalt GW4O. At 200 MPa, olivine is systematically present and the olivine-plagioclase assemblage characteristic of the glomeroporphyritic aggregates is reproduced in the near-liquidus (16 wt % crystals) experimental charge L4-1 (Table 3). In contrast, olivine is very rare in experimental products at 400 MPa. The lowest H_2O concentration needed for olivine to crystallize together with plagioclase on the 200 MPa liquidus is 5 wt% (charge P6-14, Table 3), thus providing a lower limit for the H_2O concentration in the incoming melt. For this range of melt H_2O concentration, GW4O has a liquidus temperature estimated at ~1025°C (Sisson & Grove, 1993; Pichavant & Macdonald, 2007) which is taken as the maximum temperature of the arrival magma. The minimum temperature is 975°C since amphibole is not a phenocryst phase in GW4O. Experimental olivine and plagioclase crystallized at 200 MPa, 1000°C, for a melt H_2O concentration of 5-6 wt %, have Fo between 74 and 84 and An between 87 and 88 (charges L4-1 and P6-14, Table 3), close to compositions in the glomeroporphyritic aggregates (Fo75 and An90). The most Fo-rich compositions (84-85) reflect the oxidizing fO_2 (~NNO+2) of the P6 charges, also marked in the chemistry of magnetite (Mt_{89-90}, Table 3). In comparison, the L1-1, L2-1 and L4-1 charges are less oxidizing. They yield magnetites between Mt_{74} and Mt_{77}, in the range of GW4O crystals (Mt_{73-79}) and, so, their fO_2 (ΔNNO = +1 to +1.2) is considered appropriate for the arrival magma. It is worth noting that the melt in charge L4-1 is a mafic basaltic andesite (53 wt % SiO_2, Table 3).

Conditions in the resident magma can be deduced both from geothermometry and from the andesite experiments. It is noted here that all 1530 AD products carry the same phenocryst assemblage, and that plagioclase, orthopyroxene, clinopyroxene and magnetite phenocrysts have "average" compositions common to all eruption products (see above). Therefore, conditions of chemical equilibration between liquid and crystals in the resident magma are buffered by the phenocryst assemblage and its composition. Hereafter, this buffered equilibrium state, which results from the time-integrated evolution of the andesitic reservoir, will be designated as "secular" equilibrium (e.g., Touboul et al., 2007). Below, we

Downloaded from https://academic.oup.com/petrology/advance-article-abstract/doi/10.1093/petrology/egy030/4938631
by CNRS - ISTO user
on 19 March 2018

first constrain the conditions of this equilibrium state before examining, in a second step, the perturbating influence of the incoming basaltic magma.

T-fO_2 conditions of Fe-Ti oxide equilibration were determined for magnetite and ilmenite pairs in O1215Eb and O1215B2, after checking for Mg and Mn equilibration (Bacon & Hirschmann, 1988). Both the QUILF (Andersen *et al*., 1993) and the Fe-Ti oxide geothermobarometer (Ghiorso & Evans, 2008) were used. Tightly grouped, although substantially different, equilibrium temperatures were obtained, 870-891°C with QUILF and 953-972°C with the Fe-Ti oxide geothermobarometer (Table 5). In comparison, the fO_2 values are in close agreement between the two methods (~NNO+1, Table 5). T-fO_2 results are identical, whether calculated using Fe-Ti oxide compositions from Semet *et al.* (1981) or from this study.

QUILF two-pyroxene thermometry (Andersen *et al*., 1993) was also tested to further constrain the temperature. For O1215Eb, when using "common" orthopyroxene and clinopyroxene compositions, tightly grouped temperatures were obtained, between 900 and 952°C, on average 927°C (n = 12). For the other samples, similar temperatures were obtained if the calculations were performed on the same pyroxene compositional groups, for example 933-995°C, on average 950°C (n = 8) for O1215G. However, the significance of these temperatures is unclear. Pyroxenes can be xenocrystic in the 1530 AD products and also in GW4O. Additionally, clinopyroxenes in the 1530 AD products are systematically more CaO- and Wo-rich than clinopyroxene at equilibrium with orthopyroxene in the andesite experiments. It is possible that the clinopyroxenes in the 1530 AD products are of basaltic origin (inherited from "old" mixing events) and did not completely equilibrate in the andesitic magma.

Plagioclase, orthopyroxene and magnetite compositions in the andesite experiments have been regressed as a function of temperature, pressure, melt H_2O concentration and ΔNNO. The empirical regressions enable us to use the phenocryst compositions to precisely constrain the conditions of secular equilibrium in the andesitic reservoir, and to test further the hypothesis of mutual equilibrium between phenocrysts (Table 6). Results are illustrated in Fig. 10a for plagioclase and 10b and 10c for orthopyroxene. Assuming a pressure of 170 MPa (more fully justified below), an initial ΔNNO = +0.8 and plagioclase rim compositions between An_{60} and An_{65}, pre-eruptive temperatures between 850 and 900°C, centered on 875°C, are obtained (Fig. 10a). Although both orthopyroxene and magnetite are less sensitive to temperature than plagioclase, the same temperature range (centered on 850-875°C) is obtained for the "common" orthopyroxene group (En_{56-59}, Fig. 10b; Table 6). In this

Downloaded from https://academic.oup.com/petrology/advance-article-abstract/doi/10.1093/petrology/egy030/4938631
by CNRS - ISTO user
on 19 March 2018

temperature range, and for the same melt H_2O concentrations, experimental magnetites (Mt_{66-67}) are identical to the main phenocryst group (Table 6). Strong fO_2 constraints are provided by orthopyroxene (and magnetite) compositions which indicate a pre-eruptive ΔNNO intermediate between 0 and +1 (Fig. 10c), thus providing an *a posteriori* justification of the initial choice of ΔNNO (+0.8) above (Table 6). We conclude that the compositions of the three major phenocryst phases reflect their mutual equilibration with a melt containing between 5 and 5.5 wt % H_2O, at a temperature of ~875°C and for an optimum ΔNNO of +0.8.

The results above critically depend on the range of melt H_2O concentrations. Given the dispersion in glass inclusion data (Fig. 8), the range chosen (5-5.5 wt % H_2O) represents no more than an estimation. However, the different samples have the same H_2O maxima ($\geq$ 5.5 wt %), suggesting that values in this range are representative of pre-eruptive melt H_2O concentrations (see Martel *et al.*, 2000 for similar data and conclusions for Mt. Pelée). In addition, sensibility tests using regressions of the andesite experimental data show that, with a melt H_2O concentration of 4 wt %, calculated phase compositions and proportions are inconsistent with the natural products (Table 6). Therefore, values < 5 wt % underestimate the pre-eruptive melt H_2O concentration. In comparison, a slight increase (to 6 wt %) of the melt H_2O concentration above the preferred range does not generate marked inconsistencies with the eruption products (Table 6).

At 170 MPa, 875°C, 5.5 wt % H_2O in the melt and ΔNNO =+0.8, the interstitial melt has SiO_2 = 70 wt % (Table 6). The experimental crystallinity is 55 wt %, consistent with modal data for the 1530 AD eruption products (51-65 wt %, Table 6). This provides an *a posteriori* confirmation that the andesite starting material used could be representative of a magmatic liquid. For the interstitial melt to reach a SiO_2 content more representative of glass inclusions (> 71.5-72 wt %, Fig. 5) and matrix glasses (> 70 wt %, Fig. 6), temperatures < 875°C and as low as 825°C are necessary (Table 6; n.b., melt H_2O concentrations and pressure are fixed in the calculations). Thus, the reservoir experienced temperatures cooler than defined above for secular equilibrium. Temperatures < 875°C are allowed by orthopyroxene and magnetite compositions (Fig. 10b; Table 6), but they require plagioclase rims more sodic than the An_{60-65} range considered above. At 850°C, the interstitial melt has 72 wt % SiO_2, in the range of natural glasses, and the crystallinity is 61-65 wt % (Table 6), also in the range of the eruption products. Plagioclase is An_{59-60} (Table 6), in agreement with the An_{59} rim composition previously proposed by Semet *et al.* (1981). At 825°C, the interstitial melt has up to 73 wt % SiO_2 (Table 6). This melt is in equilibrium with an An_{57} plagioclase which, although uncommon, is a composition present in the database

Downloaded from https://academic.oup.com/petrology/advance-article-abstract/doi/10.1093/petrology/egy030/4938631
by CNRS - ISTO user
on 19 March 2018

(Supplementary Data Table s2). However, the experimental crystallinity (66 wt %) is out of the natural range and so 825°C represents a lower bound. We conclude that, for the andesitic magma body and prior to the mixing event, a temperature range between 875 and 825°C satisfies all the compositional characteristics of the phenocrysts and natural glasses in the eruption products (Fig. 9a).

Depth of the reservoir

The H_2O concentration in the glass inclusions constitutes the most robust constraint on the depth of the magma reservoir (Fig. 11). For the 5-5.5 wt % melt H_2O concentration range justified above, saturation pressures between ~1350 and ~1700 bar are obtained by combining the H_2O solubility models of Burnham (1979) and Papale *et al*. (2006), the calculations being performed at 875°C for melts represented by the glass inclusions (Table 2). Note that, if other volatile species are present in addition to H_2O, this pressure range should be increased. Average glass inclusion S concentrations in the 1530 AD products range from 322 (O1215Eb), 237 (O1215B2) to 242 ppm (O1215G), corresponding to an average $\log f S_2$ of -0.32 (Poussineau, 2005). Glass inclusions have CO_2 concentrations below detection (~20 ppm, Poussineau, 2005). Their Cl concentrations range from 2463 to 3006 ppm (Boudon *et al*., 2008, see also Semet *et al*., 1981). These results imply that the magmatic vapour phase at the reservoir level is H_2O-rich, with Cl and S as the main additional components. H_2O solubilities calculated for $a H_2O = 0.9$ are illustrated (Fig. 11) to stress the influence of these Cl and S components. In the same way, slightly increasing the melt H_2O concentration range to 6 wt % would increase the upper saturation pressure by ~30 MPa (Fig. 11).

The H_2O saturation pressures above can be used directly to infer the depth of the magma reservoir. Assuming $a H_2O = 1$ and a mean rock density of 2450 $kg.m^{-3}$ (Barnoud *et al*., 2016), minimum depths range between 5.6 and 7.1 km. An upper pressure limit is provided by the absence of amphibole in the 1530 AD eruption products. At 825°C, amphibole is stable at 150 MPa and unstable at 850°C, 190 MPa (Table 4). It is stable at 875°C, 213 MPa in the compositionally similar Mt Pelée andesites (Martel *et al*., 1999). Therefore, for a temperature of 875°C, a maximum depth for the La Soufriere reservoir can be estimated at ~200 MPa (8.5 km). Geophysical signals during the 1976-1977 crisis have suggested the possible existence of a magma chamber 5-8 km below the Soufrière summit (Pozzi *et al*., 1979). Seismic observations (Hirn & Michel, 1979) have revealed a vertical migration of hypocenters from 6 km under the volcano. Although no direct relation has been established between the 1976-1977 event and the 1530 AD eruption, the longevity of the

Downloaded from https://academic.oup.com/petrology/advance-article-abstract/doi/10.1093/petrology/egy030/4938631
by CNRS - ISTO user
on 19 March 2018

Soufrière reservoir (Touboul *et al*., 2007) would render it possible that the 1976-1977 activity was driven by a magma body emplaced in or at the same level as the 1530 AD reservoir.

The pre-eruptive state

The La Soufrière reservoir immediately before the 1530 AD eruption is illustrated in Fig. 9b. Following the incoming of the basaltic magma, the resident andesitic magma body has undergone modifications, both chemical and physical. An hybrid magma, whose main characteristics (compositional, thermal) depend on the proportion of the two end-member magmas and on their respective chemical and physical conditions (e.g., Laumonier *et al*., 2014), has been generated. The proportions of silicic and mafic products in 1530 AD deposits (Semet *et al*., 1981; Boudon *et al*., 2008) suggest that the hybrid magma was assembled by mixing approximately equal proportions of andesite and basalt (Fig. 9). This magma is continuously chemically zoned as demonstrated by the 1530 AD whole-rock data (Fig. 2). To interpret this chemical zonation, we examine below how the different components of the andesitic magma, namely crystals and glasses, reacted to the mixing event.

Leaving aside the few xenocrysts of basaltic origin (see above), the modal data show that the same phenocryst assemblage is carried unchanged by the hybrid magma, whatever the bulk-rock composition. Nevertheless, there are various indications for a perturbating role of the basaltic magma on crystals. The first concerns the An-rich layers in plagioclase phenocrysts (Fig. 3). Maximum plagioclase An contents in the andesite experiments range from 71 (925°C) to 81 (950°C, Table 4; Supplementary Data Table s7). Therefore, An > 80 spikes cannot be produced by closed-system crystallization in the andesitic reservoir. They require the involvement of an external, more calcic (i.e., high Ca/Na) and presumably basaltic, melt. Plagioclase An contents reach 89 in the basalt experiments (Table 3; Supplementary Data Table s6). Zoning profiles in plagioclase phenocrysts are thus interpreted to indicate periodic basaltic recharge of the andesitic magma body. The latest of such events corresponds to the most external An-rich layer in the plagioclase phenocrysts and is interpreted to be associated with the 1530 AD eruption. The second indication is provided by the En-rich rims on orthopyroxene phenocrysts (Fig. 4). If charges 14, 15, 16 (875°C) and 36, 37, 38 (900°C) are excluded because their fO_2 is $\geq$ 2 log units more oxidizing than the andesitic magma (Tables 4, 6), maximum En in the andesite experiments are 67-68 at 925-950°C (Table 4). In the basalt experiments, orthopyroxene is rare and the maximum En is also 68 (950°C, Table 3). Therefore, compositions $\geq$ 68 in the 1530 AD products (some are up to 74, Fig. 4; Supplementary Data Table s3; Semet *et al*., 1981; Poussineau, 2005) require the

Downloaded from https://academic.oup.com/petrology/advance-article-abstract/doi/10.1093/petrology/egy030/4938631
by CNRS - ISTO user
on 19 March 2018

involvement of a melt with a Mg# $\geq$ than that of the SG7B-1 andesite. The third indication of a thermal and chemical perturbation due to the basaltic magma is the marked core-rim zonation in magnetite phenocrysts, exclusive to the more mafic members of the eruptive sequence (see above). However, it is worth emphasizing that only a few magnetite (and a few orthopyroxene) phenocrysts exhibit compositional features as above. For plagioclase phenocrysts, An-rich layers can form an important fraction of the crystal (Fig. 3), and the internal spikes correspond to "old" mixing episodes unrelated to 1530 AD. Therefore, we conclude that, overall, the andesitic phenocrysts were little modified as a result of mixing and of their incorporation in the hybrid magma.

Compared to crystals, matrix glasses were in general more severely affected by mixing, although differences exist between samples. For the homogeneous andesitic pumices and white layers of banded pumices, matrix glass compositions range from 70 wt % to > 80 wt % SiO_2 (Fig. 6), i.e., are more evolved than for secular equilibration (70 wt % SiO_2, Table 6). Therefore, a part of the pre-1530 AD andesitic body remained preserved from the influence of the basaltic magma. The interface, in the reservoir, between this unaffected part and the hybrid magma likely corresponds to the banded pumices (Fig. 9). These reveal that mafic (and hot, see below) material from the hybrid magma (the dark layers) is advected in the andesitic magma (the white layers).

Samples with matrix glasses clearly reflecting the influence of the mixing event include scoriae and the dark layers of banded pumices. Those samples have matrix glasses with SiO_2 contents < 70 wt %, some < 65 wt % (Fig. 6). For scoriae, an inter-sample dispersion is apparent, but the fact that matrix glasses reach values substantially < 70 wt % SiO_2 (i.e., less evolved than for secular equilibration) requires addition of a mafic melt. For dark layers of banded pumices, SEM observations of matrices reveal small-scale glass heterogeneity, attributed to mixing between different melts (Fig. 7). Therefore, the hybrid magma hosted a range of compositionally contrasted melts. The most silicic (~73 wt % SiO_2, Fig. 6) approach the range in the white layers of banded pumices. The least evolved are dacitic (64-68 wt % SiO_2, Fig. 6). If experimental glass compositions are used as a thermometer (Fig. 12), the most mafic glass compositions in the dark bands and mafic scoriae imply temperatures intermediate between 925 and 950°C. We note that this temperature range is broadly consistent with mixing in equal proportions of a 1000°C basalt and an 875°C andesite (see above, Fig. 9 and Laumonier *et al.*, 2014). However, hotter and more primitive melts responsible for the origin of the An-rich layers and En-rich rims (i.e., similar to glass in charge L4-1, Table 3) must have been present, at least temporarily, in the reservoir. The

Downloaded from https://academic.oup.com/petrology/advance-article-abstract/doi/10.1093/petrology/egy030/4938631
by CNRS - ISTO user
on 19 March 2018

matrix glass dataset thus provides an incomplete record of hybrid melts. Nevertheless, the continuous chemical zonation observed in the 1530 AD products can be satisfactorily explained by a three-component mixture involving a mafic melt, a silicic melt and the phenocryst assemblage (Fig. 13). Mixing proceeded essentially by addition of a mafic melt to a variably crystallized andesite body.

MAGMATIC TIMESCALES AND VOLCANOLOGICAL IMPLICATIONS

Evidence for mixed timescales

The reservoir model presented above requires temporal constraints. Of particular interest is the estimation of the time lag between the initiation of the perturbation event (i.e., the arrival of the mafic magma batch) and the triggering of the 1530 AD eruption (the parameter t in Fig. 9), since it determines the maximum time for warning in the case of magmatic unrest of the same type as for the 1530 AD event. Various types of temporal constraints are available on the La Soufrière magma reservoir. The U-Th-Ra disequilibria results of Touboul *et al*. (2007) demonstrate long timescales (from 35 to 65 ky) for processes such as differentiation from basalt to andesite. An internal isochron has yielded an age of 35 ky, interpreted as the age of the crystals (Touboul *et al*., 2007). These relatively long timescales are consistent with the identification of "old" mixing events in plagioclase phenocrysts (Fig. 3), and with the experimental demonstration (Table 6) that the phenocryst assemblage had sufficient time to equilibrate. We therefore conclude that La Soufrière crystals witness processes taking place over long timescales.

However, there is also evidence for much shorter timescales in the 1530 AD eruption products. The En-rich rims developed on "common" orthopyroxene phenocrysts have been interpreted above as markers of basaltic recharge of the andesitic body (Fig. 4). These phenocrysts record growth of an external Mg-rich layer, followed by an episode of diffusive relaxation between the En-rich and En-poor parts of the crystal. This episode lasts for the time interval between growth of the En-rich rim and the eruption (parameter t in Figure 9). To illustrate the concept, diffusion modeling of orthopyroxene crystals (Solaro, 2017) has been performed at temperatures that bracket the range determined for banded pumices (900 and 950°C, see above). The chemical zonation across one of the two modelled crystals could be satisfactorily fitted by a 1D diffusion model, yielding a timescale of 26 days for 900°C and 10 days for 950°C. For the second analysed crystal, the chemical zonation was too steep to be

Downloaded from https://academic.oup.com/petrology/advance-article-abstract/doi/10.1093/petrology/egy030/4938631
by CNRS - ISTO user
on 19 March 2018

fitted diffusively, thus indicating shorter timescales. Although preliminary, these results are given mainly to illustrate that the hybrid magma matured for a finite time prior to being erupted. We caution against their direct use because of the small number of crystals so far analysed and the possible inaccuracy in crystal direction determination. In addition, temperature might also have varied during diffusive equilibration of rims and cores since banded pumices suggest convective advection of the hybrid magma in the andesitic body. Growth of En-rich rims presumably occurred continuously during mixing (as suggested by the contrasted results between the two analyzed orthopyroxenes) and, so, these crystals give only a minimum value of t (Fig. 9). Diffusion calculations also show that from 438 (for 900°C) to 184 (for 950°C) years would be necessary to chemically homogeneize the orthopyroxene crystal of Fig. 4, which provides an upper bound for t (Fig. 9).

Additional insight on magmatic timescales comes from the chemically heterogeneous matrix glasses in the banded pumices. Chemical heterogeneity is here the result of incomplete mixing of compositionally contrasted melts (see above). Being marked at scales < 10 μm (Fig. 7), it necessarily implies very short timescales, since diffusivities in melts are fast (e.g., Pichavant *et al*., 2007). Laumonier (2013) obtained interstitial glasses heterogeneous at scales identical to those in the banded pumices in a 50 hour mixing experiment involving dry silicic and basaltic magmas at 1170°C. Although not directly applicable to La Soufrière compositions and conditions, these results suggest that timescales of the order of 10s of hours are appropriate to generate compositional heterogeneities as in Fig. 7. This range of timescales overlaps with the duration of the 1530 AD eruption (Vincent *et al.,* 1979; Boudon *et al.,* 1988; 2008). Therefore, magma mixing was taking place during the eruption and matrix glasses in the banded pumices record at least a part of the syn-eruptive mixing processes.

Volcanological implications

Mixing has been widely held responsible for the development of instabilities in magma reservoirs (e.g., Gourgaud *et al*., 1989; Murphy *et al*., 1998; 2000; Pichavant *et al*., 2002, for Lesser Antilles examples). Early models for the 1530 AD eruption of La Soufrière have stressed the importance of the temperature increase imparted to the resident andesitic magma by the arrival of the mafic magma. Semet *et al*. (1981) considered a temperature increase of 100 to 150°C, which would translate into a fluid pressure increase of 400 to 800 bar by assuming a constant volume. Such overpressures would be likely to cause failure of the roof of the reservoir, thus triggering the eruption (Semet *et al*., 1981). Our detailed parametrization of the mixing event indeed provides support to such relatively large temperature variations

Downloaded from https://academic.oup.com/petrology/advance-article-abstract/doi/10.1093/petrology/egy030/4938631
by CNRS - ISTO user
on 19 March 2018

(see Fig. 9). An initial temperature difference of 125-175°C has been determined between the resident and the arrival magma; this temperature contrast decreases to 50-75°C (Fig. 9) as heat is exchanged and the hybrid magma is progressively assembled. Therefore, the fluid pressure increase resulting from the mixing event was most probably not instantaneous as postulated by Semet *et al*. (1981). Rather, it would depend on timescales of assembly and on the thermal evolution of the hybrid magma.

Another point that needs consideration is the volatile content of the arrival magma. Our experimental results show that the basaltic magma is H_2O-rich (> 5 wt %, Table 3). This range of H_2O contents is similar to that of other evolved (~ 4-5 wt % MgO) high alumina basalts from the Lesser Antilles (Pichavant *et al*., 2002; Pichavant & Macdonald, 2007). It is much higher than the 2 wt % H_2O considered by Allard *et al*. (2014) to model the amount of underground basaltic magma sustaining the present-day hydrothermal activity at La Soufrière. It also suggests that most if not all the plumbing system of La Soufrière hosts an exsolved fluid phase (see Pichavant & Macdonald, 2007 for an evaluation of H_2O concentrations in Lesser Antilles mafic melts). If a free fluid phase is present, fluid pressures would be buffered at near-saturation values, greatly limiting the possibility of developing large fluid overpressures in the plumbing system. The importance of hydrothermal activity at La Soufrière indicates that the magmatic system is open to gas escape at its top (e.g., Allard *et al*., 2014) which casts further doubt on the possibility of establishing significant fluid overpressures in the conduit. Therefore, our results do not support a mechanism of fluid overpressure as an eruption trigger. However, they do not rule out recharge of the andesitic reservoir as a key mechanism in the initiation of the eruption. The arrival mafic magma could operate like a rising piston (Eichelberger *et al*., 2000) as represented on Fig. 9a. For the 1530 AD eruption, Boudon *et al.* (2008) proposed that magma arrived at the surface just after the initial phreatic event. Magma ascent was at the cause of a low-volume flank collapse that subsequently led to the sub-plinian phase of the eruption (Boudon *et al.*, 2008). In this context, the conditions of supply of the arrival magma (volume, flow rate) would be critical. An exceptionally high flux of mafic magma, consistent with the continuous chemical zonation and the predominance of mafic products, is probably the key factor at the origin of the 1530 AD eruption. The phenocrysts, either unreacted or steeply zoned chemically, are also consistent with a major mafic recharge event followed, shortly after, by rupturing of the reservoir (e.g., Folch & Marti, 1998). Thus, the eruptive behaviour of the La Soufrière volcano depends on processes taking place in the middle to lower part of the Lesser Antilles arc crust.

Downloaded from https://academic.oup.com/petrology/advance-article-abstract/doi/10.1093/petrology/egy030/4938631
by CNRS - ISTO user
on 19 March 2018

CONCLUDING COMMENTS

A detailed model has been presented for the pre-eruptive evolution of the La Soufrière magma reservoir. Although closely linked to the 1530 AD eruption, certain aspects of the model (depth of the reservoir, volatile content of the basaltic magma, redox state) are of direct interest for our understanding of the current state of the volcano, presently dominated by hydrothermal activity. The model also provides a framework to interpret future unrest signals in the case of magmatic reactivation. In the evolution of La Soufrière, basaltic magma recharge stands out as a major factor controlling the dynamics of the shallow andesitic body. This process is recorded over timescales of 10-100 kyr and, so, it is expected to be repeated in future. Under certain conditions (high flux of mafic magma), remobilization of most of the shallow andesitic body will result, thus increasing the potential for a magmatic eruption. Although additional temporal constraints are needed, our results indicate that remobilization of the andesitic body can take place rapidly, on a timescale of several tens of days. Mafic magma intrusions similar to 1530 AD would likely be associated with deformation signals whose detection and monitoring is a priority for eruption forecasting at La Soufrière.

A detailed quantitative parametrization of the mixing event that dominated the evolution of the reservoir prior to the 1530 AD eruption has been presented. Results illustrate and refine current magma mixing models (e.g., Gourgaud *et al*., 1989; Eichelberger *et al*., 2000; Murphy *et al*., 2000). However, the 1530 AD La Soufrière event presents several unusual aspects that are worth being emphasized.

In terms of physical and chemical parameters, melt H_2O contents and redox states were similar for both the arrival and the resident magmas at their interaction level (~200 MPa). The experimental data on GW4O confirm previous work (Pichavant *et al*., 2002) in showing that low-MgO high alumina magmas can be parental to silicic andesites in the Lesser Antilles arc. Therefore, the two types of magmas involved in the 1530 AD mixing event were most probably cogenetic. For the mafic component, the demonstration of high melt H_2O contents has implications on the physics of the mixing process. In mixed magmas, the mafic component is commonly assumed to have a density higher than the silicic component (e.g., Wiebe, 1996). In comparison, banded pumices from the 1530 AD eruption suggest convective advection of the hybrid magma in the andesitic body. This probably was facilitated by the crystal-poor nature of the incoming basaltic magma and low melt density because of high dissolved H_2O.

Downloaded from https://academic.oup.com/petrology/advance-article-abstract/doi/10.1093/petrology/egy030/4938631
by CNRS - ISTO user
on 19 March 2018

Temperature has been precisely monitored during the evolution of the reservoir. The resident magma body was at 825-875°C prior to the mixing event. The arrival magma had a temperature of ~1000°C, significantly less than previously considered (1100°C, Semet *et al*., 1981). During the assembly of the hybrid magma, the temperature dropped to 950°C in the mafic part and increased to 875-925°C at the silicic-mafic interface. A part of the andesitic body was preserved from the influence of the basaltic magma. Matrix glasses were severely impacted but, in comparison, phenocrysts were little modified as a result of their incorporation in the hybrid magma. Despite the occurrence of An-rich layers, En-rich cores and zoned magnetites, the fact that only a few phenocrysts reacted to the mixing event is a remarkable observation. La Soufrière thus provides another example of an intermediate magma submitted to a major thermal and chemical perturbation (66% of the initial andesitic body interacted with the arrival basalt) without crystals being largely affected, because timescales separating the arrival of the mafic magma and the eruption were short (Sparks *et al.*, 1977; Pallister *et al*., 1992). La Soufrière 1530 AD thus preserves a case of "arrested" magma mixing.

Additional work is needed to quantify magmatic timescales, in particular for processes (remobilization of the andesite body) directly involved in eruptive dynamics. However, the La Soufrière 1530 AD products provide evidence for a wide range of timescales, from several 10s kyr to 10s hours. This reflects the diversity of magmatic processes in the reservoir, from basalt differentiation to syn-eruptive mixing between melts, but also the ability of glasses and crystals to record different timescales. It is hoped that the petrological framework established in this work will set the stage for the precise determination of critical temporal parameters.

ACKNOWLEDGEMENTS

M. Semet, B. Villemant and N. Metrich provided samples and whole-rock data. G. Boudon helped with field work. The GW4O sample was resurfaced thanks to H. Traineau. A. Genty, O. Rouer, P. Benoist and I. Di Carlo assisted with the acquisition of the SEM and electron microprobe data, and J.M. Bény with the FTIR analyses. We also thank R. Champallier for his contribution to the experimental part of this work and B. Scaillet, C. Martel, P. Allard, G. Boudon, J.C. Komorowski and B. Villemant for discussions. The manuscript was reviewed by G. Cooper, J. Blundy and an anonymous reviewer.

Downloaded from https://academic.oup.com/petrology/advance-article-abstract/doi/10.1093/petrology/egy030/4938631
by CNRS - ISTO user
on 19 March 2018

FUNDING

This study was initially supported by INSU DYETI "Antilles" and ANR UD "Antilles" projects coordinated by MP and C. Chauvel. The PhD thesis grant to SP was provided by the French Ministry of Higher Education and Research.

REFERENCES

Allan, A.S.R., Morgan, D.J., Wilson, C.J.N. & Millet, M.A. (2013). From mush to eruption in centuries: assembly of the super-sized Oruanui magma. *Contributions to Mineralogy and Petrology* **166**, 143-164.

Allard, P., Aiuppa, A., Beauducel, F., Gaudin, D., Di Napoli, R., Calabrese, S., Parello, F., Crispi, O., Hammouya, G. & Tamburello, G. (2014). Steam and gas emission rate from La Soufrière volcano, Guadeloupe (Lesser Antilles): implications for the magmatic supply during degassing unrest. *Chemical Geology* **384**, 76-93.

Andersen, D.J., Lindsley, D.H. & Davidson, P.M. (1993). QUILF: a PASCAL program to assess equilibria among Fe-Mg-Mn-Ti oxides, pyroxenes, olivine, and quartz. *Computer & Geosciences* **19**, 1333-1350.

Bacon, C.R. & Hirschmann, M.M. (1988). Mg/Mn partitioning as a test for equilibrium between coexisting Fe-Ti oxides. *American Mineralogist* **73**, 57-61.

Barclay, J., Rutherford, M.J., Carroll, M.R., Murphy, M.D., Devine, J.D., Gardner, J.E. & Sparks, R.S.J. (1998). Experimental phase equilibria constraints on pre-eruptive storage conditions of the Soufrière Hills magma. *Geophysical Research Letters* **25**, 3437-3440.

Barnoud, A., Coutant, O., Bouligand,C., Gunawan, H. & Deroussi, S. (2016). 3-D linear inversion of gravity data: method and application to Basse-Terre volcanic island, Guadeloupe, Lesser Antilles. *Geophysical Journal International* **205**, 562–574.

Boudon, G., Dagain, J., Semet, M. & Westercamp, D. (1988). Le massif volcanique de la Soufrière (département de la Guadeloupe, Petites Antilles). Carte Géologique de la France, Editions BRGM.

Boudon, G., Komorowski, J.-C., Villemant, B. & Semet, M. (2008). A new scenario for the last magmatic eruption of La Soufrière of Guadeloupe (Lesser Antilles) in 1530 A.D. Evidence from stratigraphy radiocarbon dating and magmatic evolution of erupted products. *Journal of Volcanology and Geothermal Research* **178**, 474–490.

Burnham, C.W. (1979). The importance of volatile constituents. In: H.S. Yoder (Ed.), The evolution of igneous rocks. Princeton University Press, Princeton, 439-482.

Burnham, C.W., Holloway, J.R. & Davis, N.F. (1969). Thermodynamic properties of water to 1000°C and 10000 bars. *Geological Society of America Special Paper* **132**, 96p.

Chou, I.M. (1978). Calibration of oxygen buffers at elevated P and T using the hydrogen fugacity sensor. *American Mineralogist* **63**, 690-703.

Downloaded from https://academic.oup.com/petrology/advance-article-abstract/doi/10.1093/petrology/egy030/4938631
by CNRS - ISTO user
on 19 March 2018

Costa, F., Scaillet, B. & Pichavant, M. (2004). Petrological and experimental constraints on the pre-eruption conditions of Holocene dacite from Volcan San Pedro (36°s, chilean Andes) and the importance of sulphur in silicic subduction-related magmas. *Journal of Petrology* **45**, 1-26.

Dagain, J., Paterne, M. & Westercamp, D. (1981). La mise en place du massif volcanique Madeleine-Soufrière, Basse-Terre de Guadeloupe, Antilles. *Comptes Rendus de l'Académie des Sciences* **292**, 921-926.

Di Carlo, I., Pichavant, M., Rotolo, S. G. & Scaillet, B. (2006). Experimental crystallization of a high-K arc basalt: the golden pumice, Stromboli volcano (Italy). *Journal of Petrology* **47**, 1317-1343.

Devine, J.D., Gardner, J.E., Brack, H.P., Layne, G.D. & Rutherford, M.J. (1995). Comparison of microanalytical methods for estimating H_2O contents of silicic volcanic glasses. *American Mineralogist* **80**, 319-328.

Dohmen, R., Ter Heege, J.H., Becker, H. W. & Chakrabortry, S. (2016). Fe-Mg interdiffusion in orthopyroxene. *American Mineralogist* **101**, 2210-2221.

Eichelberger, J. C. (1978). Andesites in island arcs and continental margins: relationships to crustal evolution. *Bulletin of Volcanology* **41-4**, 480-500.

Eichelberger, J. C., Chertkoff, D. G., Dreher, S. T. & Nye, C. J. (2000). Magmas in collision: rethinking chemical zonation in silicic magmas. *Geology* **28**, 603-606.

Feuillard, M., Allègre, C.J., Brandeis, G., Gaulon, R., Le Mouel, J.L., Mercier, J.C., Pozzi, J.P. & Semet, M.P. (1983). The 1975–1977 crisis of La-Soufrière-De-Guadeloupe (FWI) — a still-born magmatic eruption. *Journal of Volcanology and Geothermal Research* **16**, 317–334.

Fichaut, M., Maury, R.C., Traineau, H., Westercamp, D., Joron, J.-L., Gourgaud, A. & Coulon, C. (1989). Magmatology of Mt. Pelée (Martinique, F.W.I.), III. Fractional crystallization versus magma mixing. *Journal of Volcanology and Geothermal Research* **38**, 189-213.

Folch, A. & Marti, J. (1998). The generation of overpressure in felsic magma chambers by replenishment. *Earth and Planetary Science Letters* **163**, 301–314.

Ganguly, J. & Tazzoli, V. (1994). Fe^{2+} - Mg^{2+} interdiffusion in orthopyroxene: retrieval from the data on intercrystalline exchange reaction. *American Mineralogist* **79**, 930-937.

Ghiorso, M. S. & Evans, B.W. (2008). Thermodynamics of rhombohedral oxide solid solutions and a revision of the Fe-Ti two-oxide geothermometer and oxygen-barometer. *American Journal of Science* **308**, 957-1039.

Gourgaud, A., Fichaut, M. & Joron, J.-L. (1989). Magmatology of Mt. Pelée (Martinique, F.W.I.), I. Magma mixing and triggering of the 1902 and 1929 pelean nuées ardentes. *Journal of Volcanology and Geothermal Research* **38**, 143-169.

Hildreth, W. (1981). Gradients in silicic magma chambers: implications for lithospheric magmatism. *Journal of Geophysical Research* **86**, 10153-10192.

Hirn, A. & Michel, B. (1979). Evidence of migration of main shocks during major seismo-volcanic crises of la Soufrière (Guadeloupe, Lesser Antilles) in 1976. *Journal of Volcanology and Geothermal Research* **6**, 295-304.

Jaupart, C. & Allègre, C.J. (1991). Gas content, eruption rate and instabilities of eruption regime in silicic volcanoes. *Earth and Planetary Science Letters* **102**, 413–429.

Kokelaar, B.P. (2002). Setting, chronology and consequences of the eruption of Soufrière Hills Volcano, Montserrat (1995-1999). In Druitt, T.H., Kokelaar, B.P. (Ed.), The eruption of Soufrière Hills Volcano, Montserrat, from 1995 to 1999. *Geological Society of London Memoir*, **21**, 1-43.

Downloaded from https://academic.oup.com/petrology/advance-article-abstract/doi/10.1093/petrology/egy030/4938631
by CNRS - ISTO user
on 19 March 2018

Laumonier, M. (2013). Mélange de magmas à HP-HT : contraintes expérimentales et application au magmatisme d'arc. PhD thesis, Université d'Orléans, 316 p.

Laumonier, M., Scaillet, B., Pichavant, M., Champallier, M., Andujar, J. & Arbaret, L. (2014). On the conditions of magma mixing and its bearing on the conditions of andesite production in the crust. *Nature Communications* **5**, 5607.

Macdonald, R. & Hawkesworth, C., Heath, E. (2000). The Lesser Antilles Volcanic chain: a study in arc magmatism. *Earth Science Reviews* **49**, 1-76.

Martel, C. (1996). Conditions pré-éruptives et dégazage des magmas andésitiques de la Montagne Pelée (Martinique) : étude pétrologique et expérimentale. PhD thesis, Université d'Orléans, 249 p.

Martel, C., Pichavant, M., Bourdier, J., Traineau, H., Holtz, F. & Scaillet, B. (1998). Magma storage conditions and control of eruption regime in silicic volcanoes : experimental evidence from Mt. Pelée. *Earth and Planetary Science Letters* **156**, 89-99.

Martel, C., Pichavant, M., Holtz, F., Scaillet, B., Bourdier, J. & Traineau, H. (1999). Effects of fO_2 and H_2O on andesite phase relations between 2 and 4 kbar. *Journal of Geophysical Research* **104**, 453-470.

Martel, C., Bourdier, J., Pichavant, M. & Traineau, H. (2000). Textures, water content and degassing of silicic andesites from recent plinian and dome-forming eruptions at Mount Pelée volcano (Martinique, Lesser Antilles arc). *Journal of Volcanology and Geothermal Research* **96**, 191-206.

Murphy, M. D., Sparks, R. S. J., Barclay, J., Carroll, M. R., Lejeune, A.-M., Brewer, T. S. et al. (1998). The role of magma mixing in triggering the current eruption at the Soufriere Hills volcano, Montserrat, WI. *Geophysical Research Letters* **25**, 3433–3436.

Murphy, M. D., Sparks, R. S. J., Barclay, J., Carroll, M. R. & Brewer, T. S. (2000). Remobilization of andesite magma by intrusion of mafic magma at the Soufriere Hills volcano, Montserrat, West Indies. *Journal of Petrology*, **41**, 21-42.

Ohlhorst, S., Behrens, H. & Holtz, F. (2001). Compositional dependence of molar absorptivities of near-infrared OH- and H_2O bands in rhyolitic to basaltic glasses. *Chemical Geology* **174**, 5-20.

Pallister, J.S., Hoblitt, R.P. & Reyes, A.G. (1992). A basalt trigger for the 1991 eruptions of Pinatubo volcano. *Nature* **356**, 426-428.

Papale, P., Moretti, R. & Barbato, D. (2006). The compositional dependence of the saturation surface of H2O + CO2 fluids in silicate melts. *Chemical Geology* **229**, 78-95.

Pichavant, M. (1987). Effects of B and H_2O on liquidus phase relations in the haplogranite system at 1kbar. *American Mineralogist* **72**, 1056-1070.

Pichavant, M., Martel, C., Bourdier, J. & Scaillet, B. (2002). Physical conditions, structure, and dynamics of a zoned magma chamber: Mount Pelée (Martinique, Lesser Antilles arc). *Journal of Geophysical Research* **107(B5),** 10.1029/2001JB000315.

Pichavant, M., Costa, R.F., Burgisser, A., Scaillet, B., Martel, C. & Poussineau, S. (2007). Equilibration scales in silicic to intermediate magmas - Implications for experimental studies. *Journal of Petrology* **48**, 1955-1972.

Pichavant, M. & Macdonald, R. (2007). Crystallization of primitive basaltic magmas at crustal pressures and genesis of the calc-alkaline igneous suite: experimental evidence from St Vincent, Lesser Antilles arc. *Contributions to Mineralogy and Petrology* **154**, 535-558.

Downloaded from https://academic.oup.com/petrology/advance-article-abstract/doi/10.1093/petrology/egy030/4938631
by CNRS - ISTO user
on 19 March 2018

Poussineau, S., (2005). Dynamique des magmas andésitiques: approche expérimentale et pétrostructurale; application à la Soufrière de Guadeloupe et à la Montagne Pelée. PhD thesis, University of Orléans, 295 pp.

Pownceby, M. & O'Neill, H. (1994). Thermodynamic data from redox reactions at high temperature. III. activity-composition relations in Ni-Pd alloys from EMF measurements at 850-1250K, and calibration of the NiO+Ni-Pd assemblage as a redox sensor. *Contributions to Mineralogy and Petrology* **116**, 327-339.

Pozzi, J., Le Mouel, J., Rossignol, J. & Zlotnicki, J. (1979). Magnetic observations made on la Soufrière Volcano (Guadeloupe) during the 1976-1977 crisis. *Journal of Volcanology and Geothermal Research* **5**, 217-237.

Rutherford, M., Sigurdsson, H., Carey, S. & Davis, A. (1985). The May 18, 1980, eruption of Mount St. Helens 1. melt composition and experimental phase equilibria. *Journal of Geophysical Research* **90**, 2929-2947.

Samper, A., Quidelleur, X., Komorowski, J.-C., Lahitte, P. & Boudon, G. (2009). Effusive history of the Grande Découverte volcanic complex, southern Basse-Terre (Guadeloupe, French West Indies) from new K-Ar Cassignol-Gillot ages. *Journal of Volcanology and Geothermal Research* **187**, 117-130.

Scaillet, B. & Evans, B. (1999). The 15 June 1991 eruption of Mount Pinatubo. I. phase equilibria and pre-eruption P-T-fO_2-fH_2O conditions of the dacite magma. *Journal of Petrology* **40**, 381-411.

Scaillet, B., Pichavant, M., Roux, J., Humbert, G. & Lefevre, A. (1992). Improvements of the Shaw membrane technique for measurement and control of fH_2 at high temperatures and pressures. *American Mineralogist* **77**, 647-655.

Scaillet, B., Pichavant, M. & Roux, J. (1995). Experimental crystallization of leucogranite magmas. *Journal of Petrology* **36**, 663-705.

Scaillet, S., Pichavant, M. & Cioni, R. (2008). Upward migration of Vesuvius magma chamber over the past 20000 years. *Nature* **455**, 216-219.

Semet, M., Vatin-Perignon, N., Vincent, P. M. & Joron, J.L. (1981). L'éruption volcanique du XVIème siècle de la Soufrière de la Guadeloupe : mélange de magmas et dynamisme éruptif. *Bulletin PIRPSEV-CNRS* **60**, 63 p.

Sisson, T. W., and Grove, T. L. (1993). Temperatures and H_2O contents of low-MgO high-alumina basalts. *Contributions to Mineralogy and Petrology* **113**, 167-184.

Solaro, C. (2017). Timescales of reservoir and degassing processes: Application to Dominica (Lesser Antilles Arc). PhD thesis, Université Paris Diderot (Paris 7), Sorbonne Paris Cité.

Sparks, S.R.J., Sigurdsson, H. & Wilson, L. (1977). Magma mixing: a mechanism for triggering acid explosive eruptions. *Nature* **267**, 315-318.

Stolper, E.M. (1982). Water in silicate glasses : an infrared spectroscopic study. *Contributions to Mineralogy and Petrology* **81**, 1-17.

Silver, L.A. & Stolper, E. (1989). Water in albitic glasses. *Journal of Petrology* **30**, 667 709.

Taylor, J., Wall, V. & Pownceby, M. (1992). The calibration and application of accurate redox sensors. *American Mineralogist* **77**, 284-295.

Tazieff, H. (1977). La Soufrière : volcanology and forecasting. *Nature* **269**, 96-97.

Downloaded from https://academic.oup.com/petrology/advance-article-abstract/doi/10.1093/petrology/egy030/4938631
by CNRS - ISTO user
on 19 March 2018

Touboul, M., Bourdon, B., Villemant, B., Boudon, G. & Joron, J.-L. (2007). ^{238}U-^{230}Th-^{226}Ra disequilibria in andesitic lavas of the last magmatic eruption of Guadeloupe Soufrière, french Antilles: processes and timescales of differentiation. *Chemical Geology* **246**, 181-206.

Traineau, H., Westercamp, D. & Coulon, C. (1986). Mé1anges magmatiques à la Montagne Pelée (Martinique) - Origine des éruptions de type Saint-Vincent. *Bulletin of Volcanology* **46**, 243-269.

Vincent, P., Vatin-Perignon, N., Semet, M. & Cheminée, J. (1979). Le dôme de la Soufrière (Guadeloupe) : son âge et son mode de mise en place. *Comptes Rendus de l'Académie des Sciences* **288**, 51-54.

Wiebe, R.A. (1996). Mafic-silicic layered intrusions: the role of basaltic injections on magmatic processes and the evolution of silicic magma chambers. *Transactions of the Royal Society of Edinburgh: Earth Sciences* **87**, 233-242.

FIGURE CAPTIONS

Fig. 1. Location of Guadeloupe Island in the Lesser Antilles Arc and simplified geological map of southern Basse-Terre showing the La Soufrière dome and the La Citerne and L'Echelle scoria cones.

Fig. 2. Major element (Al_2O_3, Fe_2O_3, MgO, K_2O) SiO_2 variation diagrams for the 1530 AD eruption products and older scoria cones (L'Echelle and La Citerne). Data from this study are shown with filled symbols and those from Dagain *et al*. (1981), Semet *et al*. (1981), Metrich (2004, personal communication), Semet (2004, personal communication) and Boudon *et al*. (2008) with open symbols. Note the distinctive composition of the pce77 sample (Semet *et al*. 1981, see also text).

Fig. 3. Representative electron microprobe profiles (from rim to rim for profiles in (a) and (b) and from core to rim for profile in (c) in plagioclase phenocrysts from the 1530 AD eruption products, showing variations in An content. (a) plagioclase in O1215Eb (white layer), (b) plagioclase in O1215B2 (pumice) and (c) plagioclase in O1215G (dark scoria). See Supplementary Data Table s1 for details about the samples.

Downloaded from https://academic.oup.com/petrology/advance-article-abstract/doi/10.1093/petrology/egy030/4938631
by CNRS - ISTO user
on 19 March 2018

Fig. 4. Inversely zoned orthopyroxene phenocryst from a dark layer in banded pumice SG11A. (a) SEM back-scattered photomicrograph. (b) Results of the electron microprobe traverse whose location is shown with a black straight line in (a). Notice the sharp inverse chemical zonation. Mg# = at. Mg / (Mg + Fe) calculated with total Fe as FeO.

Fig. 5. Compositions of glass inclusions in the 1530 AD samples. The electron microprobe data are recalculated on an anhydrous basis. Large bold symbols refer to data from this study for O1215Eb (white layer), O1215B2 (pumice), O1215G (dark scoria), whereas the data from Boudon *et al*. (2008), designated as B *et al*. 2008, are shown with smaller symbols for O1215Eb (white layer) and for various dark scoriae. The data from Semet *et al*. (1981), designated as S *et al*. 1981, are shown as squares. For this study and Boudon *et al*. (2008), the same color coding is used, blue for banded pumices, red for homogeneous pumices and green for dark scoriae. See Supplementary Data Table s1 for details about the samples. To facilitate comparison, the SiO_2 scales in this figure and in Fig. 6 are identical.

Fig. 6. Compositions of matrix glasses in 1530 AD samples. The electron microprobe data are recalculated on an anhydrous basis. Large bold symbols refer to data from this study (banded pumices SG11A and O1215Eb, pumices O1215B2 and SG7B-1, dark scoriae O1215G, SG3), whereas the data from Boudon *et al*. (2008), designated as B *et al*. 2008, are shown with smaller symbols (banded pumice O1215Ea and O1215Eb, various dark scoriae). The data from Semet *et al*. (1981), designated as S *et al*. 1981, are shown as squares. For this study and Boudon *et al*. (2008), the same color coding as in Fig. 5 is used, blue for banded pumices, red for homogeneous pumices and green for scoriae. For banded pumices, the open symbols refer to white layers and the shaded symbols to dark layers. See Supplementary Data Table s1 for details about samples.

Fig. 7. SEM photomicrograph of the matrix in a dark layer of banded pumice SG11A showing small-scale (< 10 μm) chemical heterogeneity in the glass phase, interpreted to result from mixing between melts of contrasted composition. Glass compositions are given in Table 2 and plotted in Figs. 6 and 14. Plagioclase (Plag) and orthopyroxene (Opx) microlites are also present in the matrix. Notice the important gas fraction (bubbles).

Fig 8. Histograms of the H_2O concentration in glass inclusions for the O1215Eb (banded pumice, white layer), O1215B2 (pumice), O1215G (dark scoria) and SG5A-2 (pumice)

Downloaded from https://academic.oup.com/petrology/advance-article-abstract/doi/10.1093/petrology/egy030/4938631
by CNRS - ISTO user
on 19 March 2018

samples. For samples O1215Eb, O1215B2 and O1215G, the inclusions are hosted in either plagioclase or orthopyroxene phenocrysts and the data are obtained with the modified "by difference" method. For sample SG5A-2, the inclusions are exclusively hosted in plagioclase phenocrysts and the data are FTIR analyses. Average H_2O contents of matrix glasses in O1215Eb, O1215B2 and O1215G (Table 2) are shown for comparison.

Fig. 9. Schematic representation of the two main, successive evolutionary stages considered in this study for the La Soufrière reservoir. **A**. Early remobilization. An andesite magma body is being remobilized by the arrival of a basaltic magma batch. Compositions of the andesite and basalt are assumed to be ~62 and ~50 wt % SiO_2, respectively (see text). Initial proportions of andesitic and basaltic magmas are estimated at 60 and 40 % by weight, respectively (see text). The white rectangles represent the phenocryst assemblage (plagioclase, orthopyroxene, magnetite, clinopyroxene) in the andesitic magma. Note that their density is not proportional to the crystal content. However, their number slightly increases with depth to illustrate the observed trend in modal proportions (Table 1). The temperatures indicated are constrained from experimental data on GW4O basalt and SG7B-1 andesite (see text). **B**. Pre-eruptive state. An hybrid magma has been assembled by mixing approximately 50 % basalt with 50 % andesite by weight. This leaves 20 % by weight of unaffected andesite, assumed to correspond to the roof part of the reservoir. The interface between the unaffected part and the hybrid magma is marked by banded pumices, represented by the grey-green layered box on the right. The phenocryst assemblage is kept virtually unchanged in the hybrid magma. Modifications induced by the mafic melt, represented as purple rims on the white rectangles, are minor (see text). The hybrid magma is chemically zoned from ~55-56 to ~62 wt % SiO_2 (Table 1) as a result of addition of a mafic melt to the andesitic body. The temperatures indicated are constrained from experimental data on SG7B-1 andesite and GW4O basalt (see text). t represents the time separating the situation represented in A from that represented in B, i.e., the time interval between mafic recharge and eruption.

Fig. 10. (a) and (b). Constraints on pre-eruptive temperature based on (a) regression of An (%) in plagioclase and (b) regression of En (%) in orthopyroxene *vs* melt H_2O content (wt %) in the andesite experiments. See Table 6 and Supplementary Data Table s7 for details about the regressions. The four isotherms (825, 850, 875 and 900°C) shown as continuous lines are calculated at a fixed pressure (170 MPa) and ΔNNO (+0.8) from the regressions.

Downloaded from https://academic.oup.com/petrology/advance-article-abstract/doi/10.1093/petrology/egy030/4938631
by CNRS - ISTO user
on 19 March 2018

Experimental data points are shown as diamonds of a specific colour for each isotherm. However, direct comparison between isotherms and experimental data points requires caution because the experiments have not been performed exactly under the conditions used to calculate the isotherms. Ranges of melt H_2O concentration in glass inclusions (MI), of plagioclase phenocryst rim and of "common" orthopyroxene compositions are shown as bold squares in (a) and (b**)**. Intersection with the four isotherms defines the range of pre-eruptive temperatures. (c) Constraints on pre-eruptive fO_2 based on the regression of En (%) in orthopyroxene *vs* melt H_2O content (wt %) in the andesite experiments. See Table 6 and Supplementary Data Table s7 for details about the regression. The four oxy-isobars (ΔNNO = 0, +1, +2 and +3) shown as continuous black lines are calculated at a constant pressure (150 MPa) and temperature (900°C). The data points plotted, shown as green diamonds, only come from 900°C and ~150 MPa experimental charges, each labelled with ΔNNO (Table 4). Ranges of melt H_2O concentration in glass inclusions (MI) and of "common" orthopyroxene compositions are shown as a bold square. Intersection with the four oxy-isobars defines the range of ΔNNO values. Note that, in the diagram, pressure (150 MPa) and temperature (900°C) are both slightly different from the "optimum" conditions for secular equilibration (170 MPa and 875°C, see text). However, conclusions regarding ΔNNO remain unchanged because, at fixed fO_2, En in orthopyroxene varies little with T (see (b)) and is nearly insensitive to P.

Fig. 11. Depth of the La Soufrière reservoir. See text for the justification of the range of pre-eruptive H_2O concentrations (5-5.5 wt %) from the glass inclusion data. For H_2O concentrations in this range, minimum saturation pressures between 135 and 170 MPa are obtained (aH_2O = 1, solid curves) by using a temperature of 875°C and the compositions of the glass inclusions from Table 2. This converts to minimum depths for the reservoir between 5.6 and 7.1 km, using a crustal density of 2450 km/m^3 (Barnoud *et al*., 2016). Increasing the pre-eruptive melt H_2O concentrations to 6 wt % would increase the saturation pressure by ~30 MPa, from 170 to 200 MPa. Note that the two H_2O solubility models used (Burnham, 1979; Papale *et al*., 2006) yield results very close from each other. H_2O solubilities, calculated for aH_2O = 0.9 (dashed curve) to stress the presence of chlorides and sulphur-bearing components in the magmatic gas phase, lead to deepening of the reservoir. However, amphibole would be stable above 200 MPa at 875°C (see text). Consequently, the lack of amphibole in the eruption products provides an upper limit for the depth of the reservoir (dashed black horizontal line).

Downloaded from https://academic.oup.com/petrology/advance-article-abstract/doi/10.1093/petrology/egy030/4938631
by CNRS - ISTO user
on 19 March 2018

Fig. 12. CaO *vs* SiO_2 plot for mafic (Table 2) and experimental glasses (Tables 3-4; Supplementary Data Tables s6-s7). The mafic glass data are for dark layers in banded pumices and dark scoriae. For clarity, the data for dark scoria O1215G (see Fig. 6) and from Semet *et al*. (1981) have not been plotted. Banded pumice samples: SG11A (this study) and O1215Ea (Boudon *et al*. (2008), designated as B *et al*. 2008). Dark scoria samples: Boudon *et al*. (2008). Data from this study are plotted with larger symbols than those from Boudon *et al*. (2008). Experimental glasses plotted are all from the andesite charges (+) except one basaltic charge (x, L1-1, Table 3). They have been filtered for their H_2O contents, all having between 5 and 5.5 wt % H_2O except one at 925°C (6 wt % H_2O, Table 4) and one at 950°C (L1-1, 5.8 wt % H_2O, Table 3). Note that the two 950°C charges from the andesite and basalt experiments plot remarkably close to each other. The most mafic natural glass plots intermediate between the 925 and 950°C experimental glasses.

Fig. 13. Interpretation of the chemical zonation in the 1530 AD eruption products. The proportion of crystals (wt %) in natural and experimental products is plotted as a function of their wt % SiO_2. Black symbols: 1530 AD products; green symbols: basalt GW4O experiments (Bas exps); red symbols: andesite SG7B-1 experiments (And exps). For the 1530 AD products, the data are from Table 1 (Magmas: whole-rock SiO_2; crystal proportions are modal proportions converted in wt %, see Table 6), Table 2 (Melts: matrix glass SiO_2, crystal proportions = 0%) and from Table 1 and Supplementary Data Tables s2-s5 (Crystals: calculated bulk SiO_2, crystal proportions = 100%). Only point-counted samples are considered (see Table 1). In addition, the most mafic matrix glass in the database (Boudon *et al*., 2008) is plotted together with the most silicic (Table 2). Two samples are detailed, O1215Eb (white layer, banded pumice) and O1215G (dark scoria). Three experimental charges are plotted, one for the basalt (L4-1, Table 3) and two for the andesite (SG1, SG32, Table 4). All data (Magmas: SG7B-1 glass SiO_2, crystal proportions = experimental crystallinities; Melts: experimental glass SiO_2, crystal proportions = 0%; Crystals: calculated bulk crystal SiO_2, crystal proportions = 100%) are from Tables 3 and Supplementary Data Table s6 (Bas exps) and from Tables 4 and s-7 (And exps). For the three experimental charges, the lines (small dashes) emphasize that the three components, Melts, Magmas and Crystals are aligned. This indicates that the synthetic magmas are effectively made up of binary mixtures of interstitial glass plus crystals. For the natural products, some samples (O1215Eb, others) behave similarly to experimental charges. However, others (O1215G,

Downloaded from https://academic.oup.com/petrology/advance-article-abstract/doi/10.1093/petrology/egy030/4938631
by CNRS - ISTO user
on 19 March 2018

O1215B2) plot to the left of their corresponding Melts-Crystals tie line (small dashes), thus indicating the involvement of a third component. This third component is a mafic melt derived from the arrival basaltic magma, represented by the L4-1 charge. Notice the compositional difference between the most mafic matrix glass found in banded pumices and dark scoriae and the L4-1 glass. Notice also that O1215G plots on the mixing line (long dashes) drawn between the phenocryst assemblage and the most mafic glass. This further illustrates that a melt component more mafic than the matrix glass analyzed in this sample is necessary to account for its bulk rock characteristics.

Downloaded from https://academic.oup.com/petrology/advance-article-abstract/doi/10.1093/petrology/egy030/4938631
by CNRS - ISTO user
on 19 March 2018

Table 1. Selected chemical and modal compositions

La Soufrière 1530 AD eruption												L'Echelle scoria cone		
#	SG5A-1[a]	SG5A-2[a]	SG5A-3[a]	SG6A-1[a]	SG7B-1[a]	SG7B-1	SG3[a]	O1215Eb[b]	O1215Ea[b]	O1215B2[b]	O1215G[b]	SG2[a]	GW4O[c]	GW4O
Type[d]	pumice	pumice	pumice	pumice	pumice	exp glass	dark scoria	white layer	dark layer	pumice	dark scoria	dark scoria	dark scoria	exp glass
wt.%														
SiO_2	57.7	59.54	59.24	58.42	60.99	60.4(3)[f]	57.1	60.11	56.28	56.79	56.26	51.47	50.60	51.1(4)[f]
TiO_2	0.62	0.62	0.62	0.65	0.62	0.66(8)	0.65	0.62	0.69	0.68	0.73	0.77	1.00	1.06(8)
Al_2O_3	17.93	17.44	17.50	17.52	16.84	17.3(2)	18.04	16.95	17.91	17.94	17.62	20.52	19.40	19.8(2)
Fe_2O_3	8.13	7.65	7.75	8.05	7.53	-	8.21	7.74	8.80	8.76	9.30	9.62	8.90	-
FeO	-	-	-	-	-	7.11(18)	-	-	-	-	-	-	-	9.78(3)
MnO	0.16	0.15	0.15	0.16	0.15	0.16(5)	0.16	0.16	0.17	0.17	0.18	0.18	0.19	0.12(9)
MgO	3.16	2.80	2.88	2.96	2.68	2.94(15)	3.58	2.73	3.95	3.58	4.00	3.70	5.42	5.24(15)
CaO	7.42	6.86	7.00	7.26	6.45	7.39(8)	7.82	6.60	8.30	7.73	8.12	7.44	9.90	9.75(24)
Na_2O	3.02	3.09	3.06	3.02	3.17	3.08(10)	2.91	3.07	2.70	2.82	2.79	2.82	2.63	2.91(15)
K_2O	0.88	0.96	0.93	0.91	1.09	0.94(8)	0.83	1.01	0.72	0.80	0.73	0.34	0.30	0.30(4)
P_2O_5	0.12	0.10	0.09	0.10	0.12	-	0.11	0.11	0.09	0.12	0.10	0.14	0.11	-
LOI	0.67	0.60	0.60	0.76	0.17	-	0.40	0.70	0.20	0.42	0.00	2.82	-	-
Total	99.81	99.81	99.82	99.81	99.81	100	99.81	99.80	99.81	99.81	99.83	99.82	98.45	100
Modal compositions[e] vol. %														
Gdm	-	-	44.7	42.5	51.7	-	-	54.0 (59.1)	-	49.4	40.0 (60.9)	-	65.1	-
Ol	-	-	-	-	-	-	-	-	-	-	-	-	3.6	-
Plag	-	-	42.0	43.3	36.3	-	-	35.2 (25.5)	-	38.1	43.4 (24.8)	-	22.3	-
Opx	-	-	10.0	9.9	8.9	-	-	7.8 (10.1)	-	9.3	12.1 (9.1)	-	-	-
Cpx	-	-	1.8	2.6	1.8	-	-	1.8 (2.6)	-	1.8	3.1 (2.1)	-	8.7	-
Ox	-	-	1.5	1.7	1.3	-	-	1.2 (2.7)	-	1.4	1.6 (3.1)	-	0.3	-
Total	-	-	100	100	100	-	-	100 (100)	-	100	100 (100)	-	100	-

Chemical data are whole-rock analyses for eruption products and electron microprobe analyses for experimental (exp) glasses.

[a] Data from this study. Major elements by ICP-AES. Total Fe either as Fe_2O_3 (natural samples) or as FeO (experimental glasses).

[b] From Boudon *et al.* (2008).

[c] From Dagain *et al.* (1981).

[d] See Supplementary DataTable s1 for details about samples.

[e] Point counting data (this work) are compared with modal compositions calculated by mass balance (numbers in brackets, Boudon *et al*., 2008). Gdm, groundmass, Ol, olivine, Plag, plagioclase, Opx, orthopyroxene, Cpx, clinopyroxene, Ox, magnetite and ilmenite.

[f] Compositions of experimental glasses are average of multiple electron microprobe analyses normalized to 100%.

Downloaded from https://academic.oup.com/petrology/advance-article-abstract/doi/10.1093/petrology/egy030/4938631
by CNRS - ISTO user
on 19 March 2018

Table 2. Representative compositions of glass inclusions and matrix glasses in 1530 AD eruption products.

	Glass inclusions						Matrix glasses								
wt%	O1215Eb[a]		O1215B2[b]		O1215G[c]		O1215Eb[a]	O1215B2[b]		O1215G[c]	SG11A[d]			SG3[e]	SG7B1[f]
	Plag	Opx	Plag	Opx	Plag	Plag					dark	dark	white		
SiO_2	74.51	75.26	73.92	72.6	74.49	74.42	73.79	72.7	73.48	71.64	67.42	73.81	74.87	73.01	79.69
TiO_2	0.45	0.45	0.51	0.44	0.37	0.52	0.38	0.49	0.86	0.67	0.79	0.60	0.37	0.54	0.27
Al_2O_3	12.41	11.96	13.58	13.08	12.73	12.46	12.00	12.7	12.84	12.77	14.30	13.19	12.33	12.76	11.31
FeO	3.23	2.71	2.77	3.93	3.78	4.36	4.89	4.85	4.45	4.82	6.02	3.92	3.42	4.60	1.46
MnO	nd	nd	nd	nd	nd	nd	0.61	0	0.24	0.25	0.23	0.13	0.20	0.09	0.09
MgO	0.60	0.50	0.48	0.99	0.26	0.21	0.40	0.77	0.73	0.83	1.34	0.80	0.61	0.84	0.02
CaO	2.66	2.71	2.8	2.9	2.23	1.97	2.31	3.03	3.59	3.04	4.80	3.31	2.56	3.35	0.45
Na_2O	4.18	4.33	3.86	4.05	3.94	3.80	3.71	3.52	1.59	3.74	3.38	2.10	3.13	2.58	1.82
K_2O	1.95	2.07	2.07	2.01	2.20	2.27	1.91	1.94	2.13	2.07	1.56	2.07	2.34	2.16	4.90
P_2O_5	nd	nd	nd	nd	nd	nd	nd	nd	0.10	nd	0.15	0.05	0.18	0.07	0.00
Total	92.51	95.35	92.41	92.24	92.48	94.45	97.24	100.4	95.90	99.02	98.20	96.4	98.90	95.70	94.10
H_2O (wt%)	5.3	2.5	5.4	5.6	5.5	3.4	1.1	0.9	nd	1.0	nd	nd	nd	nd	nd
S (ppm)	245	nd	224	250	296	424	nd	nd	nd	nd	nd	nd	nd	nd	nd

Electron microprobe data normalized to 100% anhydrous. Original unnormalized Total is reported. Total Fe as FeO.
For glass inclusions, the nature of the host mineral is specified: Plag, plagioclase, Opx, orthopyroxene.
H_2O contents estimated with the modified by difference method (see text). For matrix glasses, average values are given.
[a] banded pumice, white layer.
[b] homogeneous pumice.
[c] dark scoria.
[d] banded pumice, dark means analysis in a dark layer and white analysis in a white layer.
[e] dark scoria.
[f] homogeneous pumice.
See also Supplementary Data Table s1 for details about samples.

Downloaded from https://academic.oup.com/petrology/advance-article-abstract/doi/10.1093/petrology/egy030/4938631
by CNRS - ISTO user
on 19 March 2018

Table 3. Conditions and results of the basalt experiments.

Charge	H_2O melt wt%	logfO_2 MPa	ΔNNO	Phase assemblage	SiO_2 melt wt%	An Plag	Fo Ol	En Opx	Mg# Cpx	Mg# Amph	Mt Mt
Run L1, 217.6 MPa, 950°C, fH_2 = 0.33 MPa, 72 hours											
L1-1	5.8[a]	-9.9	+1.2	Gl(39)[d], Amph(17), Opx(7) Mt(5), Plg(32)	61.9	78	-	68	-	69	77
Run L2, 226.7 MPa, 975°C, fH_2 = 0.41 MPa, 48 hours											
L2-1	6.3[a]	-9.6	+1.1	Gl(57), Amph(12), Ol(4) Cpx(tr), Plg(23), Mt(4)	58.9	85	72.4	-	75	73	74
Run L4, 204.2 MPa, 1000°C, fH_2 = 0.44 MPa, 24 hours											
L4-1	5.9[a]	-9.3	+1.0	Gl(84), Ol(3), Plg(12), Mt(1)	53	88	74.4	-	-	-	75
Run P6, 203.2 MPa, 999°C, fH_2 = 0.09 MPa, 18 hours											
P6-14	5.0[b]	-8.1	+2.2	Gl(78), Ol(2), Plg(12) Cpx(2), Mt(6)	55.7	87	84.0	-	80	-	90
P6-17	4.5[b]	-8.2	+2.1	Gl(63), Ol(4), Plg(24) Cpx(3), Mt(6)	58.8	84	85.0	-	78	-	89
Run L3, 403.3 MPa, 975°C, fH_2 = 0.48 MPa, 50 hours											
L3-1	9.3[a]	-9.1	+1.5	Gl(74), Amph(22), Mt(4)	55.4	-	-	-	-	69	79
Run P5, 400.1 MPa, 995°C, fH_2 = 0.63 MPa, 23 hours											
P5-11	6.8[b]	-9.3	+1.0	Gl(89), Amph(10), Mt(1)	52.7	-	-	-	-	74	88
P5-13	6.2[b]	-9.3	+1.0	Gl(80), Amph(3), Ol(3) Plg(13), Mt(1)	53.5	87	72.1	-	-	74	74
Run P3, 399.5 MPa, 997°C, fH_2 = 0.24 MPa, 23 hours											
P3-8	4.0[b]	-9.0	+1.4	Gl(64), Plg(20), Cpx (10) Mt(6)	57.4	68	-	-	75	-	83

Downloaded from https://academic.oup.com/petrology/advance-article-abstract/doi/10.1093/petrology/egy030/4938631
by CNRS - ISTO user
on 19 March 2018

Run L5, 404.8 MPa, 1000°C, fH_2 = 0.12 MPa, 24 hours											
L5-1	8.9[a]	-7.5	+2.8	Gl(94), Mt(6)	54.5	-	-	-	-	-	96
Run L6, 404.5 MPa, 1025°C, fH_2 =0.026 MPa, 24 hours											
L6-1	8.9[a]	-5.8	+4.1	Gl(95), Mt(5)	53.7	-	-	-	-	-	97
Run P2, 399.7 MPa, 1032°C, fH_2 =0.102 MPa, 16 hours											
P2-5	3.0[b]	-10.1	-0.2	Gl(35), Plg(44), Cpx(2) Opx(17), Mt(2)	53.2	65	-	59	64	-	43
Run P4, 396.8 MPa, 1038°C, fH_2 =0.198 MPa, 17 hours											
P4-9	4.77[c]	-7.9	+1.8	Gl(98), Plg(1), Mt(1)	51.9	89	-	-	-	-	92

[a] H_2O-saturated charge. H_2O content calculated with the model of Burnham (1979).

[b] H_2O content estimated using the by-difference method.

[c] H_2O content determined by Karl-Fischer titration (Pichavant *et al*., 2002).

[d] Phase proportions calculated by mass balance; Gl, glass; Ol, olivine; Plg, plagioclase; Opx, orthopyroxene; Cpx, clinopyroxene; Sp, spinel; Mt, magnetite; Amph, amphibole; nd: not determined. tr: a trace of (phase proportion < 1% by weight). SiO_2 melt: silica content of the residual glass; An: anorthite content of plagioclase; Fo: forsterite content of olivine; En: enstatite content of orthopyroxene; Mg#: 100 atomic Mg/(Mg+Fe) of either clinopyroxene or amphibole; Mt: magnetite content of spinel (data from Supplementary Table s6).

Downloaded from https://academic.oup.com/petrology/advance-article-abstract/doi/10.1093/petrology/egy030/4938631
by CNRS - ISTO user
on 19 March 2018

Table 4. Conditions and results of the andesite experiments.

Charge	H_2O melt wt%	logfO_2 MPa	ΔNNO	Phase assemblage	SiO_2 Glass	An Plag	En Opx	Mg# Cpx	Mg# Amph	Mt Mt	Ilm Ilm
Run S15, 153 MPa, 800°C, fH_2 = 0.3 MPa, 240 hours											
SG45	~ 4.5	~ -13.2	~ +0.6	Gl, Plag, Amph, Opx, Mt	nd	nd	54	-	64	74	-
Run S4, 204 MPa, 800°C, fH_2 = 0.853 MPa, 384 hours											
SG13	6.4[a]	-13.8	+0.1	Gl(33[b]), Plag(43), Opx(7), Amp(16), Ilm(1), Mt(<1)	72.6	50	*43*	-	50	nd	90
Run S7, 152.5 MPa, 825°C, fH_2 = 0.27 MPa, 216 hours											
SG23	5.5	-12.5	+0.9	Gl(31), Plag(48), Opx(5), Amph(14), Mt(2)	74.7	59	*49*	-	52	69	-
SG29	3.4	-12.8	+0.6	Gl(19), Plag(61), Opx(18), Mt(2)	77.4	49	50	-	-	68	-
Run S3, 102 MPa, 850°C, fH_2 = 0.35 MPa, 240 hours											
SG9	4.3	-12.5	+0.4	Gl(32), Plag(52), Opx(11), Cpx(2), Mt(3)	73.4	61	57	65	-	63	-
SG10	~ 2.5	~ -13.1	~ -0.2	Gl, Plag, Opx, Mt	nd	56	48	-	-	58	-
SG11	~ 1.5	~ -13.7	~ -0.8	Gl, Plag, Opx, Mt	nd	53	46	-	-	57	-
Run S1, 149.5 MPa, 850°C, fH_2 = 0.45 MPa, 240 hours											
SG1	5.0	-12.4	+0.5	Gl(38), Plg(47), Opx(7), Cpx(5), Mt(3)	72.3	62	60	65	-	67	-
SG2	4.3	-12.5	+0.4	Gl(24), Plg(61), Opx(12), Mt(3)	74.1	60	58	-	-	65	-
SG3	3.3	-12.8	+0.1	Gl(25), Plg(58), Opx(7), Cpx(7), Mt(3)	75.1	58	55	60	-	61	-
Run S2, 190.3 MPa, 850°C, fH_2 = 0.51 MPa, 240 hours											

Downloaded from https://academic.oup.com/petrology/advance-article-abstract/doi/10.1093/petrology/egy030/4938631
by CNRS - ISTO user
on 19 March 2018

SG5	6.4	-12.3	+0.6	Gl(61), Plag(25), Opx(8), Cpx(4) Mt(2)	67.0	nd	59	67	-	63	-
SG6	5.6	-12.3	+0.6	Gl(24), Plag(60), Opx(14), Mt(2)	70.3	*56*	55	-	-	57	-
SG7	~ 4	~ -12.7	~ +0.2	Gl, Plag, Opx, Cpx, Mt	nd	56	53	?	-	56	-
Run S5, 152.5 MPa, 875°C, fH_2 = 0.04 MPa, 200 hours											
SG14	5.1	-11.2	+3.2	Gl(49), Plag(34), Opx(5), Cpx(7), Mt(5)	72.5	64	71	76	-	82	-
SG15	4.1	-11.3	+3.1	Gl (43), Plag(37), Opx(6), Cpx(9), Mt(5)	74.3	62	68	71	-	81	-
SG16	3.1	-11.6	+2.8	Gl(29), Plag(49), Opx(2), Cpx(16), Mt(4)	74.3	58	65	65	-	80	-
Run S10, 175.2 MPa, 875°C, fH_2 = 0.37 MPa, 120 hours											
SG32	5.4	-11.6	+0.8	Gl(44), Plag(41), Opx(13), Mt(2)	71.2	nd	57	-	-	67	-
SG33	4.3	-11.7	+0.7	Gl(35), Plag(47), Opx(9), Cpx(7), Mt(2)	72.3	nd	55	61	-	64	-
Run S8, 207.7 MPa, 875°C, fH_2 = 0.38 MPa, 168 hours											
SG26	6.0	-11.5	+0.9	Gl(54), Plag(31), Opx(9), Cpx(5), Mt(1)	68.1	64	57	63	-	70	-
SG27	3.6	-11.9	+0.5	Gl(36), Plag(45), Opx(10), Cpx(7), Mt(2)	71.6	59	54	60	-	67	-
SG28	3.6	-11.9	+0.5	Gl(32), Plag(50), Opx(8), Cpx(8), Mt(2)	71.7	57	54	58	-	67	-
Run S11, 156 MPa, 900°C, fH_2 = 0.02 MPa, 144 hours*											
SG36	6.0	-8.6	+3.4	Gl(49), Plag(34), Opx(5), Cpx(7), Mt(5)	*73.2*	65	79	77	-	84	-
SG37	5.3	-8.6	+3.4	Gl(31), Plag(51), Opx(7), Cpx(6), Mt(5)	*74.5*	*59*	71	75	-	82	-
SG38	4.4	-8.7	+3.3	Gl(32), Plag(51), Opx(8), Cpx(5), Mt(4)	*74.0*	nd	67	71	-	78	-
Run S12, 155.4 MPa, 900°C, fH_2 = 0.37 MPa, 168 hours*											

Downloaded from https://academic.oup.com/petrology/advance-article-abstract/doi/10.1093/petrology/egy030/4938631
by CNRS - ISTO user
on 19 March 2018

SG39	5.6	-11.2	+0.8	Gl(42), Plag(39), Opx(10), Cpx(6), Mt(3)	*72.1*	63	60	66	-	70	-
SG40	4.7	-11.2	+0.8	Gl(43), Plag(39), Opx(10), Cpx(6), Mt(2)	70.6	60	55	63	-	67	-
SG41	4.3	-11.3	+0.7	Gl(36), Plag(48), Opx(14), Mt(2)	*72.8*	nd	53	-	-	66	-
Run S16, 150.5 MPa, 900°C, fH_2 = 0.42 MPa, 100 hours											
SG48	5.7	-11.3	+0.5	Gl(42), Plag(43), Opx(14), Mt(1)	*71.2*	nd	58	-	-	62	-
SG50	~ 3.5	~ -11.6	~ +0.7	Gl, Plag, Opx, Mt	nd	nd	52	-	-	53	-
Run S14, 151.5 MPa, 900°C, fH_2 = 1.01 MPa, 168 hours*											
SG42	5.1	-12.1	-0.2	Gl(50), Plag(34), Opx(8), Cpx(6), Mt(2), Ilm(<1)	69.9	68	53	59	-	49	92
SG43	4.2	-12.2	-0.3	Gl(36), Plag(44), Opx(9), Cpx(9), Mt(2), Ilm(<1)	70.9	61	48	55	-	48	92
SG44	3.8	-12.3	-0.4	Gl(33), Plag(49), Opx(17), Ilm(1)	72.8	60	49	-	nd	50	91
Run S6, 148.5 MPa, 925°C, fH_2 = 0.3 MPa, 96 hours											
SG18	6.0	-10.4	+1.2	Gl(66), Plag(22), Opx(5), Cpx(5), Mt(2)	67.6	71	68	68	-	71	-
SG19	4.1	-10.7	+0.9	Gl(46), Plag(40), Opx(10), Cpx(2), Mt(2)	71.2	65	58	62	-	64	-
SG20	2.0	-11.1	+0.5	Gl(22), Plag(63), Opx(8), Cpx(5), Mt(2)	70.9	55	57	63	-	61	-
Run S13, 208.1 MPa, 950°C, fH_2 = 0.32 MPa, 120 hours											
SG35	6.9	-9.8	+1.3	Gl (87), Plag(8), Opx(4), Mt(1)	60.0	81	67	-	-	71	-

*****Isobaric quench; all the other experiments were drop-quenched.

[a]H_2O content estimated using the by-difference method.

[b]Phase proportions calculated by mass balance; Gl, glass; Ol, olivine; Plg, plagioclase; Opx, orthopyroxene; Cpx, clinopyroxene; Sp, spinel; Mt, magnetite; Amph, amphibole; Ilm: ilmenite; nd: not determined. tr: a trace of (phase proportion < 1% by weight). SiO_2 melt: silica content of the residual glass; An: anorthite content of

Downloaded from https://academic.oup.com/petrology/advance-article-abstract/doi/10.1093/petrology/egy030/4938631
by CNRS - ISTO user
on 19 March 2018

plagioclase; En: enstatite content of orthopyroxene; Mg#: 100 atomic Mg/(Mg+Fe) of either clinopyroxene or amphibole; Mt: magnetite content of spinel; Ilm: ilmenite content of ilmenite (data from Supplementary Table s7).
For charges SG45, 10, 11, 7 and 50, H_2O melt and logfO_2 data are approximative (glass could not be satisfactorily analysed).
Numbers in italics indicate compositional data not considered in the regressions (either SiO_2 glass, An plag or En opx).

Downloaded from https://academic.oup.com/petrology/advance-article-abstract/doi/10.1093/petrology/egy030/4938631
by CNRS - ISTO user
on 19 March 2018

Table 5. Temperatures and oxygen fugacities calculated from Fe-Ti oxide equilibria.

Sample	1215Eb[d]	1215Eb	1215Eb	1215Eb	1215Eb	1215B2[e]	1215B2[d]	1215B2[d]	pce77[a]	lca[a]
Fe-Ti oxide couple	Mt7-Ilm1	Mt6-Ilm2	Mt5-Ilm3	Mt5-Ilm2	Mt5-Ilm1	Mt10-Ilm4	Mt11-Ilm4	Mt12-Ilm4		
Calculations after Andersen *et al.*, 1993 (QUILF)										
T (°C)	890	888	889	886	885	870	891	877	862	865
ΔNNO[b]	+1.0	+1.2	+1.0	+1.2	+1.2	+1.3	+1.1	+1.2	+0.9	+1.0
Calculations after Ghiorso & Evans, 2008 (Fe-Ti oxide geothermobarometer)										
T (°C)[c]	971	964	953	967	963	970	972	966	924	918
ΔNNO	+0.9	+0.9	+0.8	+0.9	+0.9	+0.8	+0.9	+0.9	+0.7	+0.7

All calculations performed at 2000 bar.

[a] Fe-Ti oxide pairs from Semet *et al.* (1981). All other oxide pairs from Supplementary Table s5.

[b] $\Delta NNO = \log fO_{2calc} - \log fO_{2NNO}$ at the same T and P (NNO equation from Chou, 1978).

[c] Fe-Ti exchange temperature (Ghiorso & Evans, 2008).

[d] banded pumice, white layer.

[e] homogeneous pumice.

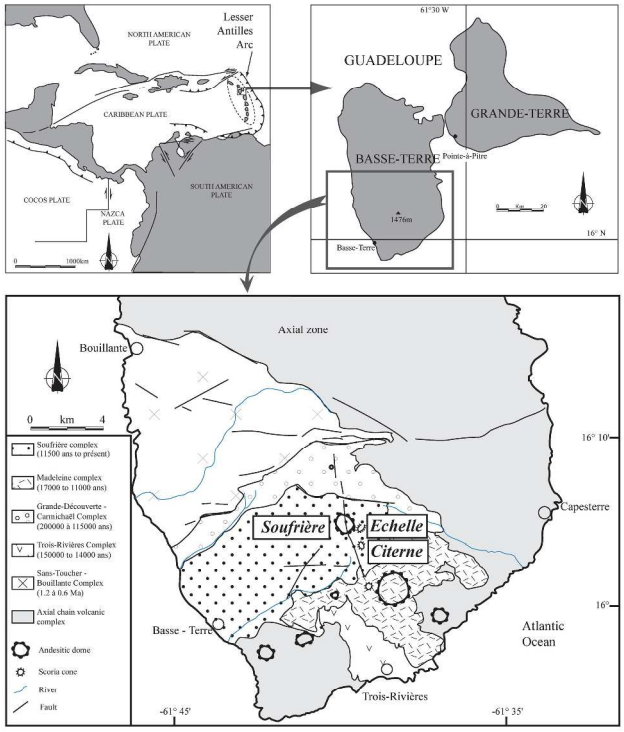
Downloaded from https://academic.oup.com/petrology/advance-article-abstract/doi/10.1093/petrology/egy030/4938631
by CNRS - ISTO user
on 19 March 2018

Table 6. Experimental constraints on the pre-eruptive conditions in the La Soufrière reservoir.

Experimental conditions				Compositional variables				
Pressure (bar)	Temperature (°C)	H_2O melt (wt%)	ΔNNO	SiO_2 melt[a] (wt%)	An[a] (%)	En[a] (%)	Mt[a] (%)	Total Ctx[a] (wt%)
Experimental charges								
1700	875	5.5	0.8	70	63	59	66	55
1700	875	5.0	0.8	71	62	58	66	59
1700	875	5.5	1.0	71	63	59	67	55
1700	850	5.5	0.8	72	60	58	67	61
1700	850	5.0	0.8	72	59	57	67	65
1700	825	5.5	0.8	73	57	57	68	66
1700	850	4	0.8	74	56	55	67	73
1700	850	6	0.8	71	62	59	67	57
Eruption products								
				64-76	60-65	56-59	66-68	51-65[b]

[a]From regressions of experimental compositions on SG7B1 (Table 4, Supplementary Data Table s7). Regression parameters are compiled in Table s8.
[b]Modal compositions (Table 1) are converted to phase proportions in wt % using densities for glass (2.4 g/cm^3), plagioclase (2.71 g/cm^3), orthopyroxene (3.6 g/cm^3), clinopyroxene (3.4 g/cm^3), Fe-Ti oxides (5.2 g/cm^3).
See Table 4 for details about compositional variables. Total Ctx = sum of plagioclase, pyroxene and Fe-Ti oxide proportions.
See text for compositions in eruption products.

Downloaded from https://academic.oup.com/petrology/advance-article-abstract/doi/10.1093/petrology/egy030/4938631
by CNRS - ISTO user
on 19 March 2018

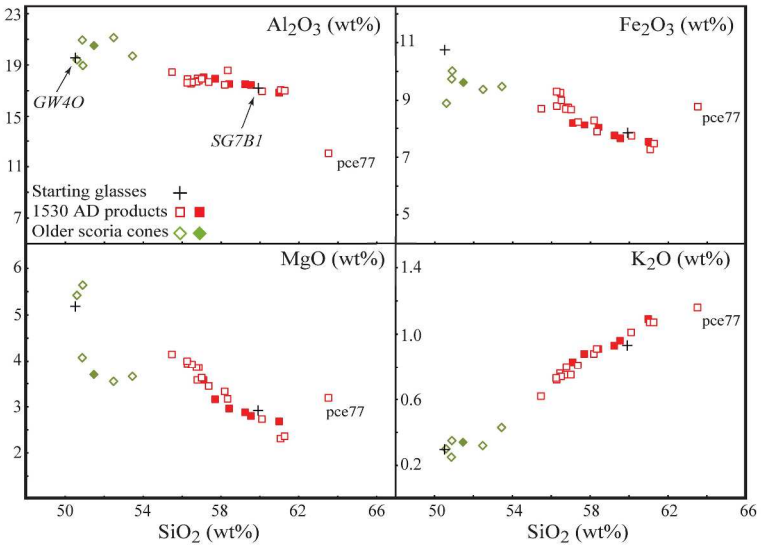


Pichavant et al., Fig. 1

Fig. 1

297x420mm (300 x 300 DPI)

Downloaded from https://academic.oup.com/petrology/advance-article-abstract/doi/10.1093/petrology/egy030/4938631
by CNRS - ISTO user
on 19 March 2018

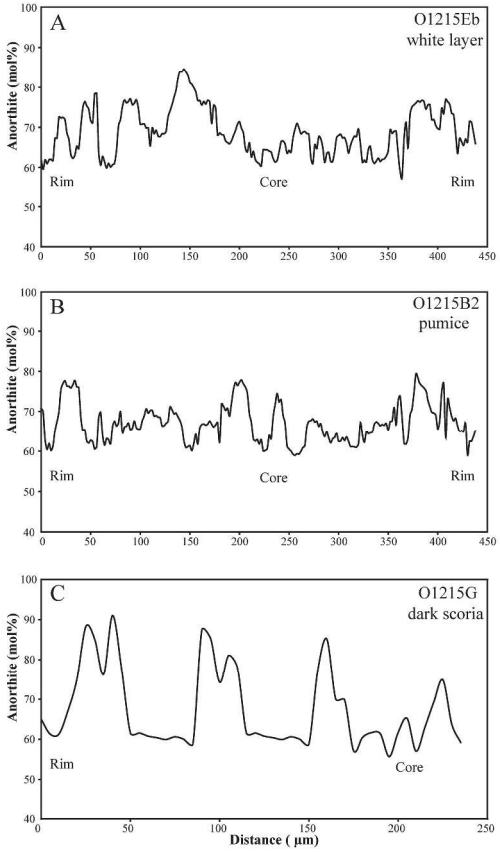


Pichavant et al., Fig. 2

Fig. 2

297x420mm (300 x 300 DPI)

Downloaded from https://academic.oup.com/petrology/advance-article-abstract/doi/10.1093/petrology/egy030/4938631
by CNRS - ISTO user
on 19 March 2018

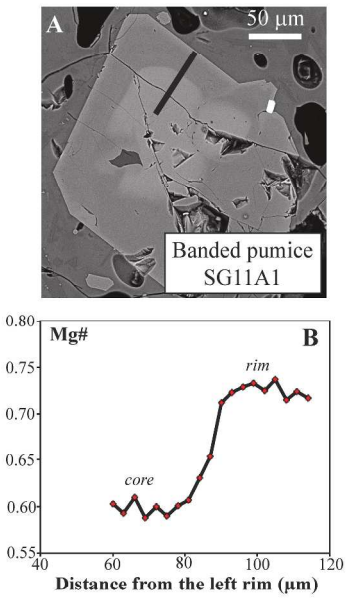


Pichavant et al., Fig. 3

Fig. 3

297x420mm (300 x 300 DPI)

Downloaded from https://academic.oup.com/petrology/advance-article-abstract/doi/10.1093/petrology/egy030/4938631
by CNRS - ISTO user
on 19 March 2018

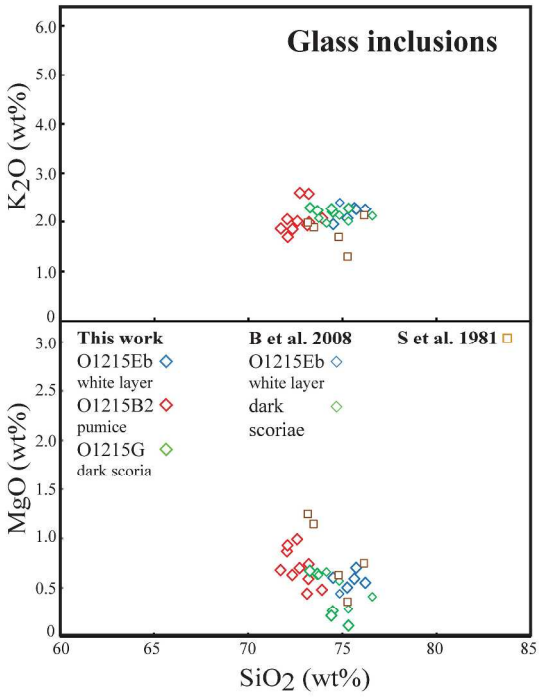


Pichavant et al., Fig. 4

Fig. 4

299x450mm (300 x 300 DPI)

Downloaded from https://academic.oup.com/petrology/advance-article-abstract/doi/10.1093/petrology/egy030/4938631
by CNRS - ISTO user
on 19 March 2018

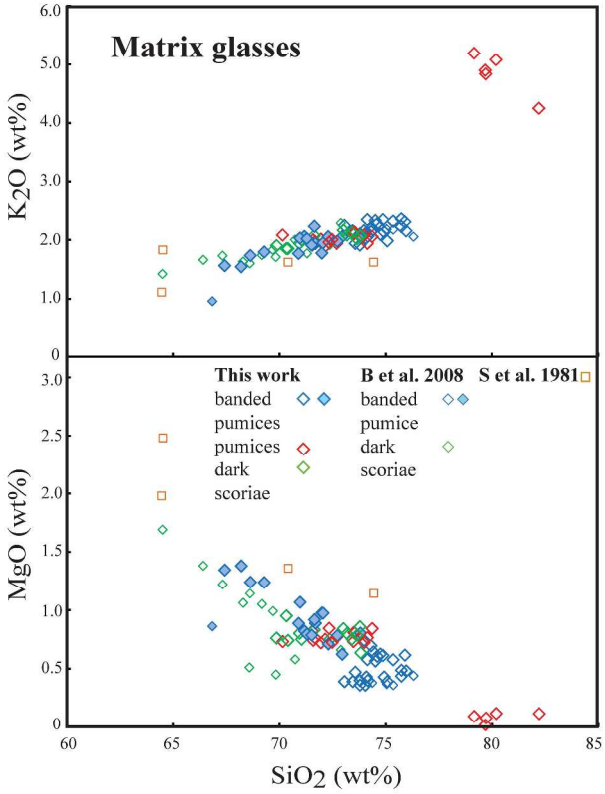


Pichavant et al., Fig. 5

Fig. 5

299x450mm (300 x 300 DPI)

Downloaded from https://academic.oup.com/petrology/advance-article-abstract/doi/10.1093/petrology/egy030/4938631
by CNRS - ISTO user
on 19 March 2018

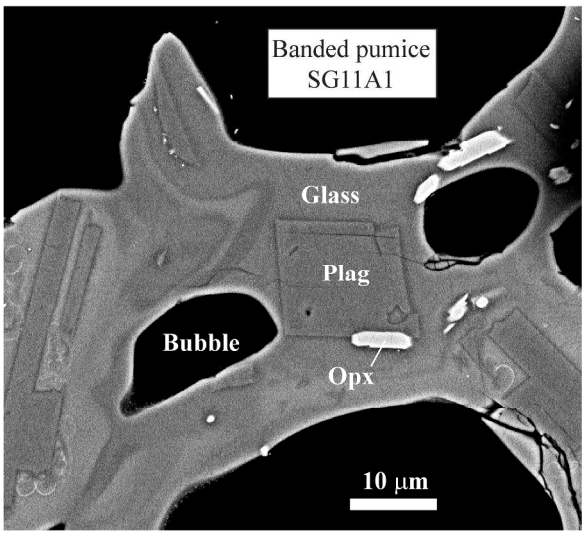


Pichavant et al., Fig. 6

Fig. 6

299x450mm (300 x 300 DPI)

Downloaded from https://academic.oup.com/petrology/advance-article-abstract/doi/10.1093/petrology/egy030/4938631
by CNRS - ISTO user
on 19 March 2018

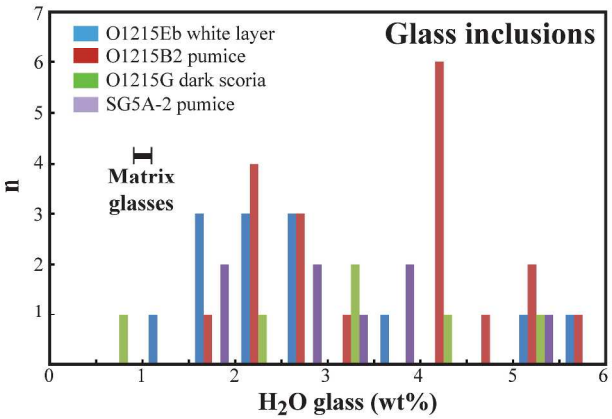


Pichavant et al., Fig. 7

Fig. 7

299x450mm (300 x 300 DPI)

Downloaded from https://academic.oup.com/petrology/advance-article-abstract/doi/10.1093/petrology/egy030/4938631
by CNRS - ISTO user
on 19 March 2018

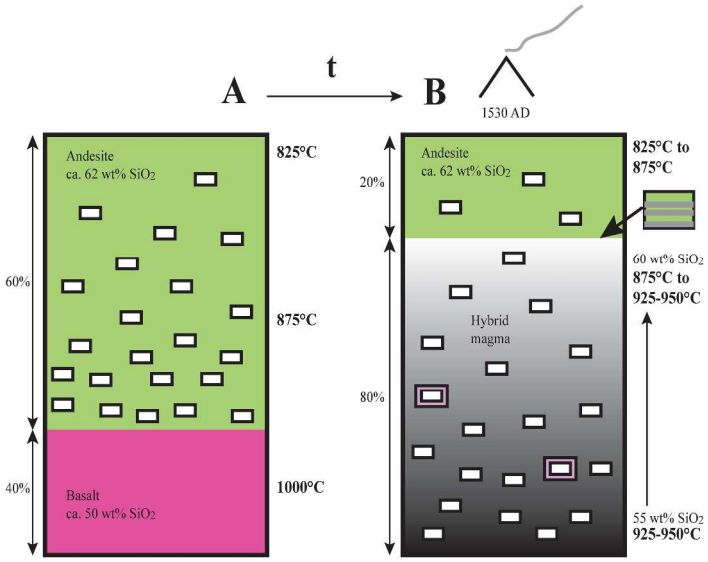


Pichavant et al., Fig. 8

Fig. 8

299x450mm (300 x 300 DPI)

Downloaded from https://academic.oup.com/petrology/advance-article-abstract/doi/10.1093/petrology/egy030/4938631
by CNRS - ISTO user
on 19 March 2018

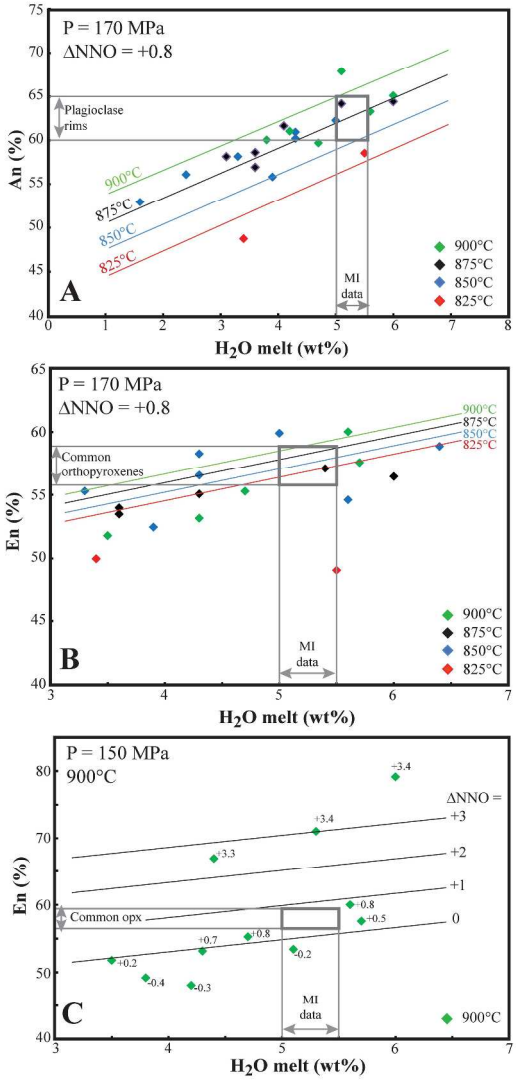


Pichavant et al., Fig. 9

Fig. 9

299x450mm (300 x 300 DPI)

Downloaded from https://academic.oup.com/petrology/advance-article-abstract/doi/10.1093/petrology/egy030/4938631
by CNRS - ISTO user
on 19 March 2018

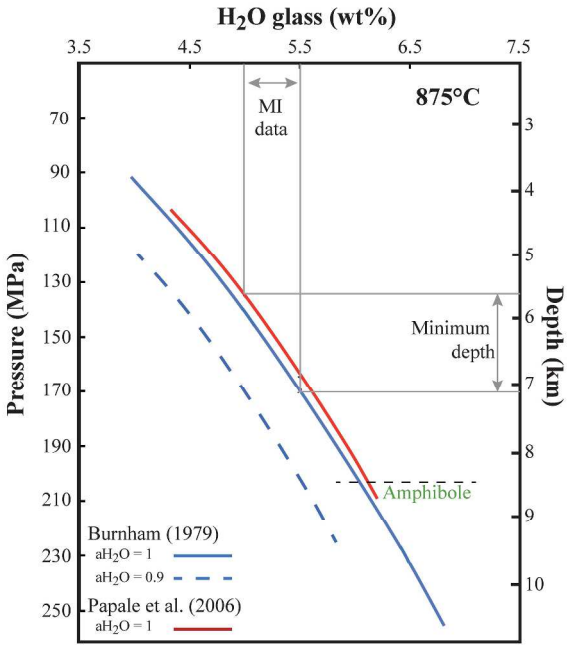


Pichavant et al., Fig. 10

Fig. 10

299x450mm (300 x 300 DPI)

Downloaded from https://academic.oup.com/petrology/advance-article-abstract/doi/10.1093/petrology/egy030/4938631
by CNRS - ISTO user
on 19 March 2018

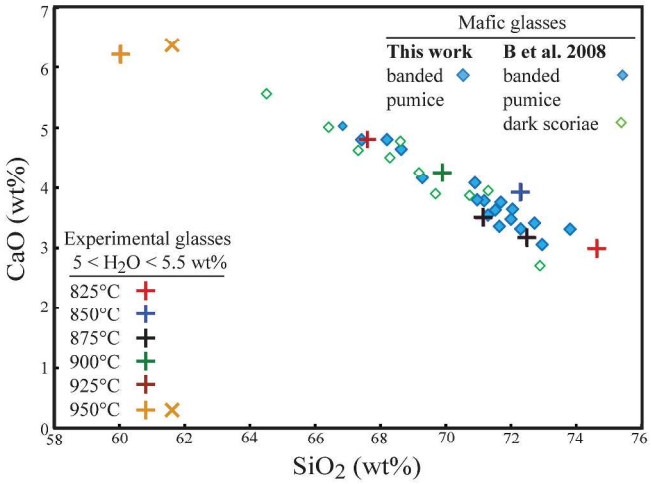


Pichavant et al., Fig. 13

Fig.11

299x450mm (300 x 300 DPI)

Downloaded from https://academic.oup.com/petrology/advance-article-abstract/doi/10.1093/petrology/egy030/4938631
by CNRS - ISTO user
on 19 March 2018

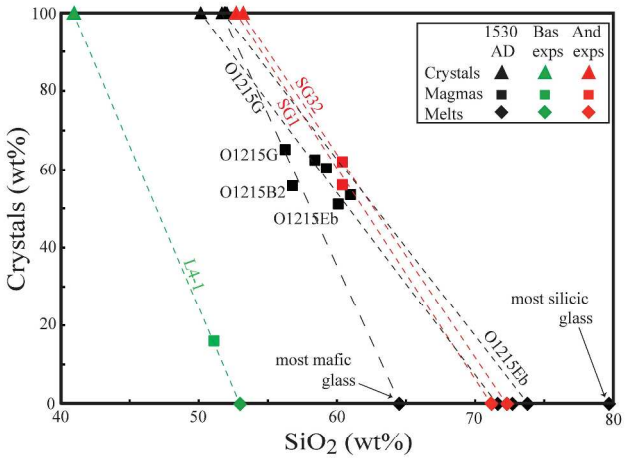


Pichavant et al., Fig. 14

Fig. 12

299x450mm (300 x 300 DPI)

Downloaded from https://academic.oup.com/petrology/advance-article-abstract/doi/10.1093/petrology/egy030/4938631
by CNRS - ISTO user
on 19 March 2018



Pichavant et al., Fig. 15

Fig. 13

299x450mm (300 x 300 DPI)

Downloaded from https://academic.oup.com/petrology/advance-article-abstract/doi/10.1093/petrology/egy030/4938631
by CNRS - ISTO user
on 19 March 2018